Electromagnetic phenomena related to a low-frequency plasma in cuprate superconductors

M. Tachiki, T. Koyama, and S. Takahashi
Institute for Materials Research, Tohoku University, 2-1-1 Katahira, Aoba-ku, Sendai 980, Japan
(Received 29 November 1993; revised manuscript received 11 April 1994)

The plasma with c-axis polarization in cuprate superconductors has a very low frequency. Experiments show that in some of the cuprate superconductors the plasma frequency is lower than the superconducting energy gap and the plasma damping is extremely weak in the superconducting state. Various electromagnetic phenomena caused by the excitation of the low-frequency plasma are studied theoretically. The reflectivity and transmissivity of the electromagnetic wave for a film of the cuprate superconductor depend strongly on the frequency and polarization of the wave and the film thickness, since the wave strongly interacts with the transverse component of the plasma. When vortices are introduced by an external magnetic field, the vortex motion and the gapless excitation in the vortex cores make the transmissivity and reflectivity strongly field dependent. The effect of the low-frequency plasma is incorporated in the ac Josephson effect. When a voltage of $(h/2e)\times$(plasma frequency) is applied to the Josephson junction of the cuprate superconductor, the plasma is excited by the ac Josephson effect and then the excited plasma will decay by emitting electromagnetic waves. The plasma excitation also affects the current-voltage characteristics of the junction.

I. INTRODUCTION

Using high-quality single crystals of $La_{2-x}Sr_xCuO_4$, Tamasaku, Nakamura, and Uchida measured the reflectivity for infrared light with c-axis polarization.[1] Their experimental data show an edge structure in the frequency range of 20–50 cm^{-1} of the reflectivity spectrum, which is assigned to originate from the plasma oscillation. The frequency of the plasma with c-axis polarization is extremely low;[1,2] the frequencies of the plasmas with the other polarizations are usually observed above 5000 cm^{-1} in cuprate superconductors.[3–8] The reasons for the low frequency of the plasma with c-axis polarization are the following. There are many pieces of experimental evidence which suggest that when charge carriers are doped in the cuprate oxides, the carriers mainly enter into the CuO_2 layers[9,10] and other layers remain semiconductive.[11–18] The interlayer transfer of the carriers through the semiconducting layers is very weak and thus the carriers are almost confined in the CuO_2 layers.[19–34] The two-dimensional nature of the electronic state is one of the reasons for the plasma in $La_{2-x}Sr_xCuO_4$ having the low frequency. Another reason is that this crystal has a large dielectric constant along the c axis.[1,35,36] This large dielectric constant works to reduce the plasma frequency.

The frequency of the plasma with c-axis polarization is smaller than the superconducting energy gap and much smaller than the optical-phonon frequencies.[1,2,37] Therefore, most of plasma damping processes are prohibited to occur in the superconducting state. According to the extremely weak plasma damping, the clear plasma edge structure in the reflection spectra is observed in the superconducting state.

Related to the weak plasma damping, many exotic electromagnetic phenomena are expected to occur in the superconducting state of the cuprate superconductors. In Sec. II we discuss the nature of the transverse plasma excited by the electromagnetic wave. By the plasma excitation, the reflectivity and transmissivity of the electromagnetic wave for a film of a cuprate superconductor strongly depend on the thickness of the film and the frequency and polarization of the electromagnetic wave. In Sec. III, we discuss how the reflectivity and transmissivity are changed by application of a magnetic field which introduces vortices in the film. If the transverse plasma is excited by some experimental method, we expect emission of the electromagnetic wave with the plasma frequency, since there is almost no decay process other than the decay to the electromagnetic wave in the superconducting state. In Sec. IV we formulate theory of the ac Josephson effect in the presence of low-frequency plasma and show that the plasma can be excited by the ac Josephson effect. The plasma excitation affects the current-voltage characteristics of the junction. In Sec. V we give a summary.

II. TRANSVERSE PLASMA AND THE REFLECTIVITY AND TRANSMISSIVITY OF THE ELECTROMAGNETIC WAVE

The penetration depth of the cuprate oxides is highly anisotropic; λ_c is much longer than λ_a and λ_b. Due to the anisotropy one branch of the plasma appears at a low frequency and the other two branches appear at much higher frequencies. We are interested in the low-frequency plasma with c-axis polarization. When the propagation directions of the plasmas are parallel to the a and c axes, the plasmas with c-axis polarization are purely transverse and longitudinal, respectively. When the propagation direction is in an intermediate direction, the plasma is a mixture of the transverse and longitudinal plasmas. However, the plasma frequency is almost in-

dependent of the propagation direction for small wave numbers. In this section we confine ourselves to the case of the transverse plasma with c-axis polarization and discuss the nature of the plasma in the superconducting state using the two-fluid model of superconductivity.[38–40]

We take the x and y axes in the ab plane of the cuprate oxide and the z axis in the direction of the c axis of the oxide. We consider a transverse plasma wave propagating in the direction of the x axis. The electric field E_z, the superconducting current J_{sz}, and the normal current J_{nz} are all parallel to the z axis, and the magnetic field is parallel to the y axis. The Maxwell equation in this case is expressed as

$$\frac{\partial}{\partial x}H_y=\frac{4\pi}{c}J_{sz}+\frac{4\pi}{c}J_{nz}+\frac{\epsilon_c}{c}\frac{\partial}{\partial t}E_z \ , \tag{2.1}$$

where ϵ_c is the dielectric constant along the c axis in the insulating phase. If the current terms in Eq. (2.1) are included in the transverse dielectric constant defined by the equation

$$\frac{\partial}{\partial x}H_y=\frac{\epsilon(\omega)}{c}\frac{\partial}{\partial t}E_z \ , \tag{2.2}$$

the dielectric constant is expressed as[38]

$$\epsilon(\omega)=\epsilon_c-\frac{\tilde{\omega}_{ps}^2}{\omega(\omega+i0^+)}-\frac{\tilde{\omega}_{pn}^2}{\omega(\omega+i\gamma)} \ , \tag{2.3}$$

with

$$\tilde{\omega}_{ps}^2=c^2/\lambda_c^2 \ , \tag{2.4}$$

and

$$\tilde{\omega}_{pn}^2=4\pi e^2 n/m^* \ , \tag{2.5}$$

where λ_c is the London penetration depth along the c axis, n is the density of thermally excited particles, m^* is the effective mass along the c axis, and γ is the scattering rate. The quantity $\tilde{\omega}_{ps}^2$ is proportional to the carrier number condensed in the superconducting state. We define $\tilde{\omega}_p^2$ by

$$\tilde{\omega}_{ps}^2+\tilde{\omega}_{pn}^2=\tilde{\omega}_p^2 \ . \tag{2.6}$$

Then, $\tilde{\omega}_p^2$ is the quantity proportional to the total number of carriers in the two-fluid model. The quantities $\tilde{\omega}_{ps}^2$ and $\tilde{\omega}_{pn}^2$ are functions of temperature and frequency. As the temperature increases, $\tilde{\omega}_{ps}^2$ decreases and $\tilde{\omega}_{pn}^2$ increases. When the frequency ω increases up to a frequency comparable to the superconducting energy gap, $\tilde{\omega}_{ps}^2$ decreases and $\tilde{\omega}_{pn}^2$ increases, since the Cooper pairs are broken into the quasiparticles. The plane-wave solution of Eq. (2.2) combined with the Maxwell equation

$$\frac{\partial}{\partial x}E_z=\frac{1}{c}\frac{\partial}{\partial t}H_y \ , \tag{2.7}$$

gives the transverse plasma wave. The dispersion relation of the transverse plasma for $\gamma=0$ is given by

$$\omega_T(k)=[(\tilde{\omega}_p^2+c^2k^2)/\epsilon_c]^{1/2} \ , \tag{2.8}$$

k being the wave number along the x axis. We see that the plasma frequency is strongly screened by ϵ_c, which is very large in cuprate superconductors.[1,35,36] As seen from the above derivation the transverse plasma is a composite wave of the electric current wave and the electromagnetic wave.

Let us consider an electromagnetic wave incident on a surface of the crystal parallel to the yz plane. We assume that the propagation vectors of the incident and reflected waves in vacuum and the plasma wave in the crystal are all parallel to the x axis, and the electric vectors of all the waves are parallel to the z axis. The electromagnetic and plasma waves are calculated by solving the Maxwell equations in vacuum and Eqs. (2.2) and (2.7) in the crystal under the boundary condition that the electric and magnetic fields of the waves are continuous at the surface. The calculation of the Poynting vectors of the incident and reflected electromagnetic waves gives the usual formula of the reflectivity

$$R=|[1-\sqrt{\epsilon(\omega)}]/[1+\sqrt{\epsilon(\omega)}]|^2 \ . \tag{2.9}$$

The frequency dependence of the reflectivity calculated by using (2.9) is shown for four temperatures in Fig. 1. The frequency of the electromagnetic wave is normalized by the plasma frequency $\omega_p=\tilde{\omega}_p/\sqrt{\epsilon_c}$. In the calculation we used the temperature dependence of $\tilde{\omega}_{ps}$ and $\tilde{\omega}_{pn}$ which is obtained in the two-fluid model. Since we do not know the temperature dependence of γ in the superconducting state, we assume a function which drastically decreases below T_c and almost vanishes below $0.6T_c$. The frequency and temperature dependence of the reflectivity shown in Fig. 1 reproduces the characteristic of the reflectivity observed in $La_{2-x}Sr_xCuO_4$. In Fig. 1 we see that the reflectivity at low temperatures has a clear dip structure just above the plasma frequency. At the dip frequency $\epsilon(\omega)$ is nearly equal to unity and thus the plasma phase velocity is nearly equal to the light velocity. Therefore, the crystal is almost transparent for the electromagnetic wave. As temperature increases, the normal component contribution of the dielectric constant from thermally excited quasiparticles increases and thus the dip structure becomes obscure. As temperature fur-

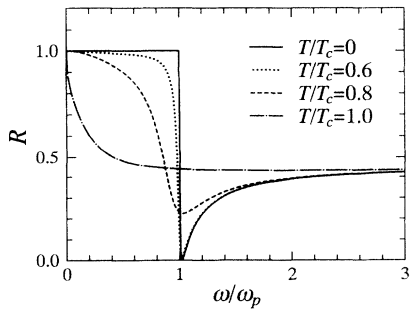

FIG. 1. Frequency dependence of the reflectivity for the crystal surface of the cuprate superconductors for several temperatures. The frequency ω is normalized by the plasma frequency ω_p.

ther increases above T_c, the dip structure completely disappears.

The frequency dependence of the reflectivity mentioned above is closely related to the nature of the plasma wave. The electric field of the plasma wave is calculated as

$$E_z = E_0 \frac{2}{1+\sqrt{\epsilon(\omega)}} \exp[i(\omega/c)\sqrt{\epsilon(\omega)}x - i\omega t] , \quad (2.10)$$

E_0 being the amplitude of the incident electromagnetic wave. The electric fields for several frequencies are calculated at absolute zero using Eq. (2.10) and are shown as functions of the distance from the surface in Fig. 2. The electric field is normalized by E_0 which is estimated to be 27.4 V/cm for an incident electromagnetic wave with power of 1 W/cm^2. The distance in Fig. 2 is normalized by c/ω_p which is estimated to be 31.8 μm for $La_{2-x}Sr_xCuO_4$ with $x=0.16$ and $\omega_p=50$ cm^{-1}. Since the dielectric constant is negative for $\omega \leq \omega_p$, the electric field for the frequency is of a standing wave with a finite penetration depth from the surface as seen from Eq. (2.10). This fact means that the electromagnetic field is perfectly reflected by the crystal. In Fig. 2 we show the amplitude of the standing wave. Both the amplitude and penetration depth of the electric field increase as the frequency increases. When the frequency approaches the plasma frequency, the penetration depth tends to infinity. When the frequency ω further increases above the plasma frequency, the dielectric constant becomes positive. For the frequency the electric field Eq. (2.10) is of a propagating wave. Therefore, the reflectivity diminishes from unity. As the frequency increases further, the transverse

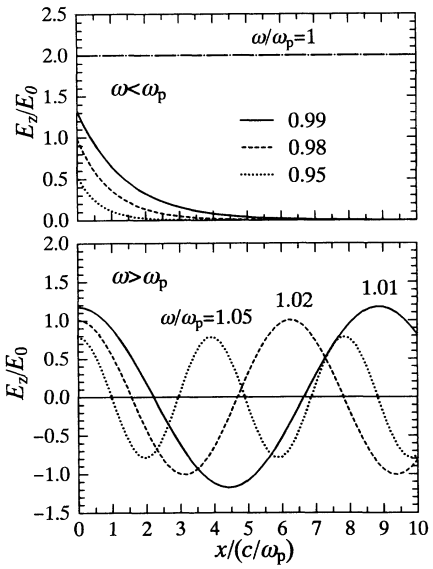

FIG. 2. Electric field normalized by the amplitude of the incident electromagnetic wave E_0 as a function of the distance from the surface. The upper figure shows the electric fields of the standing plasma waves excited by the electromagnetic waves with frequencies below the plasma frequency. The lower figure shows the electric fields of the propagating plasma waves for the electromagnetic wave with frequencies above the plasma frequency.

plasma gradually turns to a pure electromagnetic wave.

The electric current of the plasma $J_z = J_{sz} + J_{sn}$ is calculated as

$$J_z = E_0 \frac{2\sigma(\omega)}{1+\sqrt{\epsilon(\omega)}} \exp[i(\omega/c)\sqrt{\epsilon(\omega)}x - i\omega t] , \quad (2.11)$$

where $\sigma(\omega)$ is the conductivity defined by

$$\sigma(\omega) = \frac{i}{4\pi}\left[\frac{\tilde{\omega}_{ps}^2}{(\omega+i0^+)} + \frac{\tilde{\omega}_{pn}^2}{(\omega+i\gamma)}\right] . \quad (2.12)$$

The frequency dependence of the oscillating electric current is similar to that of the electric field shown in Fig. 2. The amplitude of the oscillating current is approximately 3×10^2 A/cm for an incident electromagnetic wave with power of 1 W/cm^2.

From the nature of the plasma wave discussed above, we expect that if the crystal has a finite thickness and a shape of film, the reflectivity and transmissivity of the electromagnetic wave strongly depend on the thickness of the film. The plasma wave is reflected at the surfaces of both sides of the film and the reflected plasma waves interfere with each other. The amplitudes of the plasma waves in the film and those of the electromagnetic waves in vacuum are calculated by solving Eqs. (2.2) and (2.7) in the film and the Maxwell equation in vacuum under the boundary condition at the surfaces. Calculating the Poynting vectors of the incident, reflected, and transmitted electromagnetic waves, we obtain the expressions for the reflectivity R and the transmissivity T as[41]

$$R = \left|\frac{(1-P^2)[1-\epsilon(\omega)]}{[1+\sqrt{\epsilon(\omega)}]^2-[1-\sqrt{\epsilon(\omega)}]^2P^2}\right|^2 , \quad (2.13)$$

$$T = \left|\frac{4P\sqrt{\epsilon(\omega)}}{[1+\sqrt{\epsilon(\omega)}]^2-[1-\sqrt{\epsilon(\omega)}]^2P^2}\right|^2 , \quad (2.14)$$

with

$$P = \exp[i(\omega/c)\sqrt{\epsilon(\omega)}d] , \quad (2.15)$$

where d is the thickness of the film. Using Eqs. (2.13) and (2.14), we calculate the reflectivity and transmissivity at absolute zero and show the result in Fig. 3. In the calculation, we used the parameter values for $La_{2-x}Sr_xCuO_4$ with $x=0.16$. Figure 3(a) shows the reflectivity and transmissivity for the film with thickness of 9.5 μm. The dip in the reflectivity just above the plasma frequency is one previously discussed. The dip at $\omega/\omega_p=2.32$ originates from the interference effect of the plasma waves reflected at the surfaces of the film, and half the wave length of the plasma wave coincides with the thickness of the film at the frequency. At the dip frequencies in the reflectivity, peaks appear in the transmissivity as seen in Fig. 3(a). In a thicker film of 95 μm the interference effect is more pronounced as seen in Fig. 3(b). In the calculation we assume that $\tilde{\omega}_{ps}^2$ and $\tilde{\omega}_{pn}^2$ are independent of the frequency ω. However, when ω is higher than the superconducting energy gap, $\tilde{\omega}_{ps}^2$ decreases and $\tilde{\omega}_{pn}^2$ increases according to the depairing effect of the Cooper pairs. If the effect is taken into account, for the frequencies above the superconducting energy gap [for ω/ω_p

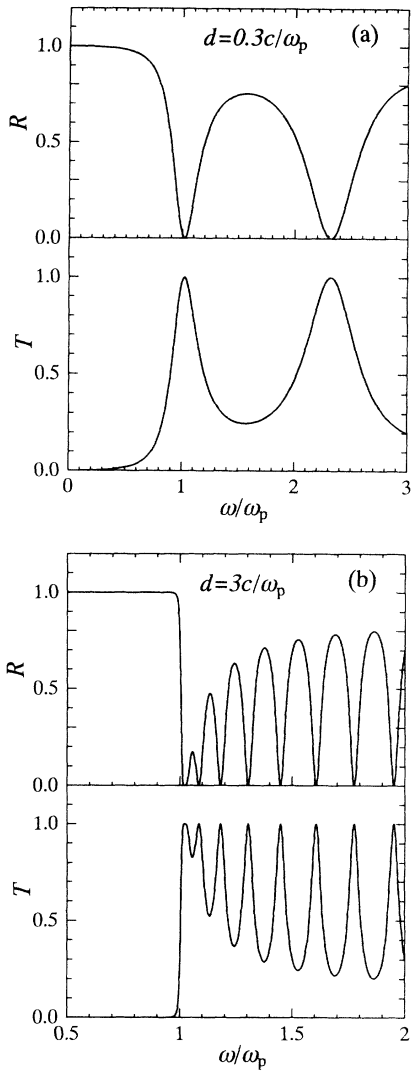

FIG. 3. Reflectivity and transmissivity of electromagnetic wave for films as functions of the frequency. The upper and lower figures in (a) and (b) show the reflectivity and transmissivity, respectively. The quantity d indicates the thickness of the film normalized by c/ω_p.

above 3 in Figs. 3(a) and 3(b)] the reflectivity should be reduced and the transmissivity should tend to the value of $|(1-\sqrt{\epsilon_c})/(1+\sqrt{\epsilon_c})|^2 \approx 0.44$.

In this paper we assume the polarization of the incident electromagnetic wave to be parallel to the c axis. When the polarization direction is tilted from the c axis, only the component of the electric field of the electromagnetic wave parallel to the c axis can pass through the film. Therefore, when the incident wave is unpolarized, the transmitted wave is changed to the wave polarized parallel to the c axis. The transmissivity of the unpolarized wave is half of the transmissivity for the wave polarized parallel to the c axis.

III. MAGNETIC-FIELD DEPENDENCE OF REFLECTIVITY AND TRANSMISSIVITY

Next we study how the reflectivity and transmissivity are changed by application of a magnetic field. The magnetic field stronger than the lower critical field H_{c1} introduces vortices into the film. The vortices effect a change of the dielectric constant of the film in two different ways. One is the effect of increase of the scattering rate due to the gapless excitation inside the vortex normal cores. The other is the effect of vortex motion driven by the oscillating current of the transverse plasma.

A. Magnetic field parallel to the c axis

When the external magnetic field is parallel to the c axis and thus the vortices are parallel to the electric current of the plasma, no Lorentz force works on the vortices. Therefore, the vortex motion is not important in this case and only the gapless excitation in the vortex cores contributes to the dielectric constant. We assume that the area of the vortex cores is in the normal state and the outside of them is in the superconducting state. The areas in the normal and superconducting states are approximately given by B_0/H_{c2} and $1-B_0/H_{c2}$, respectively, where B_0 and H_{c2} are the flux density and the upper critical field, respectively. The dielectric constant of this system at low temperatures may be written from an inspection of Eq. (2.3) as

$$\epsilon(\omega)=\epsilon_c-\frac{\tilde{\omega}_p^2}{\omega(\omega+i0^+)}\left[1-\frac{B_0}{H_{c2}}\right]-\frac{\tilde{\omega}_p^2}{\omega(\omega+i\gamma)}\left[\frac{B_0}{H_{c2}}\right]. \tag{3.1}$$

The reflectivity and transmissivity calculated by using Eq. (3.1) are shown in Fig. 4. These quantities for a relatively thin film are mildly dependent on the magnetic field as seen in Fig. 4(a), while the quantities for a thicker film are strongly changed by the magnetic field as seen in Fig. 4(b).

B. Magnetic field perpendicular to the c axis

When an external magnetic field is applied perpendicular to the c axis, the vortex cores are stabilized in the weakly superconducting layers, e.g., in the (La,Sr)O layers in $La_{2-x}Sr_xCuO_4$. Since the superconducting order parameter in the layers is primarily very small, inclusion of the vortex cores does not affect the dielectric constant so much. The main contribution to the dielectric constant in this case comes from the vortex motion in the following way. The plasma wave with c-axis polarization carries the oscillating current parallel to the c axis. The current exerts the Lorentz force on the vortices and the force causes the oscillating motion of the vortices under the influence of the vortex pinning force and the vortex viscous drag force.[42–48] In Appendix A, the dielectric constant which includes the contribution from the vortex motion is derived at low temperatures. The dielectric constant is given by

$$\epsilon_T^{zz}(\omega)=\epsilon_c-\frac{\tilde{\omega}_p^2}{\omega(\omega+i0^+)}\times\left[1+\frac{\phi_0}{4\pi\lambda_c^2}\frac{B_0}{\kappa_p-i\omega\eta-M\omega^2}\right]^{-1}, \tag{3.2}$$

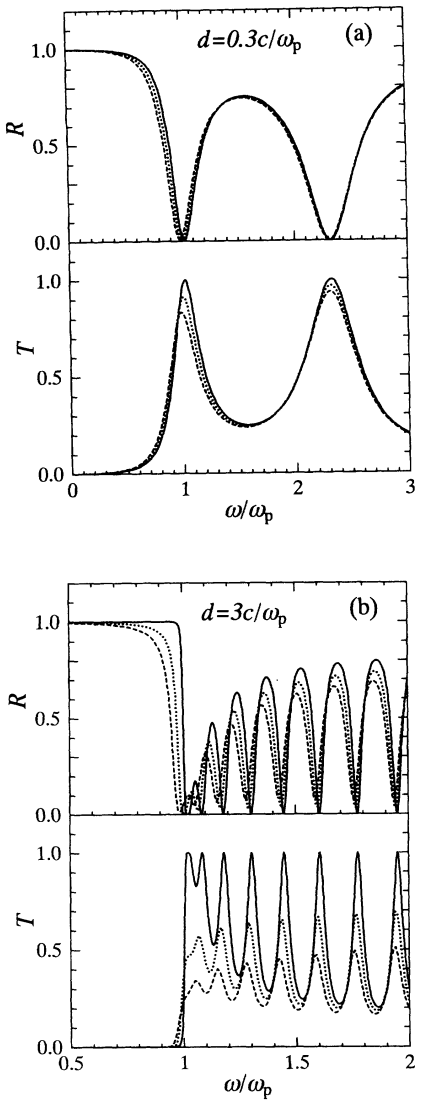

FIG. 4. Reflectivity and transmissivity of electromagnetic wave for films in magnetic fields parallel to the c axis and thus parallel to the film surface. (a) and (b) show the frequency dependence for films with thickness denoted by d. The upper and lower figures in (a) and (b) show the reflectivity and transmissivity, respectively. The solid, dotted, and dashed curves indicated the quantities in the magnetic fields of 0, 0.04, and 0.08 in units of H_{c2}, respectively. The frequency and thickness are normalized by ω_p and c/ω_p, respectively.

where ϕ_0 is the unit flux, B_0 is the flux density, κ_p and η are the pinning-force and viscous drag-force coefficients, respectively, and M is the vortex inertial mass per unit length. The dielectric constant Eq. (3.2) is rewritten as

$$\epsilon_T^{zz}(\omega)=\epsilon_c-\frac{\tilde{\omega}_p^2}{\omega(\omega+i0^+)}\times\left[1+\frac{B_0}{H_{c2}}\frac{\tau_v/\tau_n}{1-i\omega\tau_v-M\omega^2/\kappa_p}\right]^{-1}, \quad (3.3)$$

where the quantities τ_n and $\tau_v=\eta/\kappa_p$ are the relaxation times for the normal electron and the vortex motion, respectively. In deriving Eq. (3.3) we used the Bardeen-Stephen model[48] in which η is given by $H_{c2}/(c^2\rho_n)$, ρ_n being the normal electron resistivity. We assume $\rho_n=\rho_c,\rho_c$ being the normal electron resistivity along the c axis. In the calculation of the reflectivity and transmissivity we use the dielectric constant Eq. (3.3) and take the values of $B_0/H_{c2}=0$, 0.01, and 0.02, $\tau_n/\tau_v=0.1$, $\tau_n\tilde{\omega}_p=1$, and $M\tilde{\omega}_p^2/\kappa_p=0$. The result is shown in Fig. 5. The reflectivity and transmissivity especially for the thick film is strongly diminished by application of the magnetic field as seen in Fig. 5(b).

The mechanism of the diminution of the reflectivity and transmissivity by the magnetic field differs depending on whether the magnetic field is applied parallel or per-

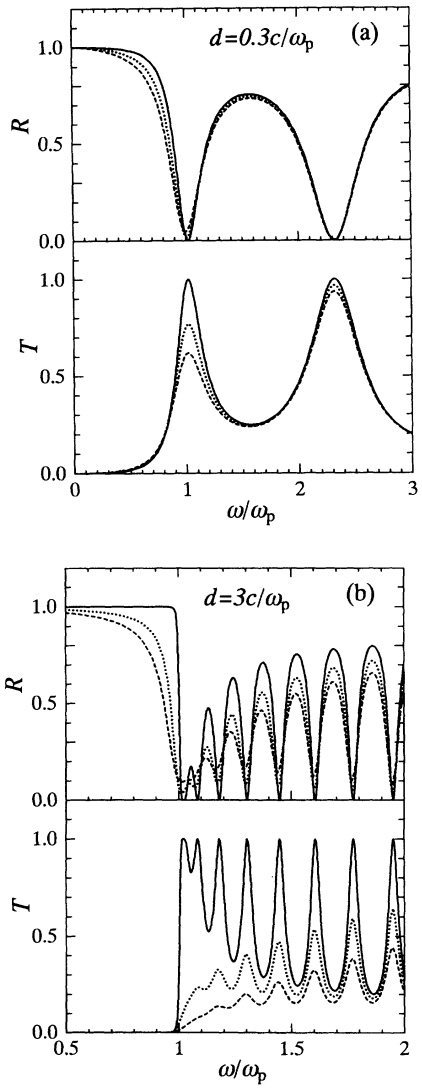

FIG. 5. Reflectivity and transmissivity of electromagnetic wave for films in magnetic fields parallel to the CuO_2 planes. (a) and (b) show the frequency dependence for films with thickness denoted by d. The upper and lower figures in (a) and (b) show the reflectivity and transmissivity, respectively. The solid, dotted, and dashed curves indicate the quantities in the magnetic fields of 0, 0.01, and 0.02 in units of H_{c2}, respectively. The frequency and thickness are normalized by ω_p and c/ω_p, respectively.

pendicular to the c axis as discussed in the Secs. III A and III B. Therefore, the magnetic-field dependence of the reflectivity and transmissivity generally differs depending on the direction of the external magnetic field.

IV. PLASMA EXCITATION BY JOSEPHSON EFFECT

In this section we investigate the effect of the low-frequency plasma on the ac Josephson effect and show that the plasma can be excited by the oscillating current generated by the ac Josephson effect. Let us consider a Josephson junction of a cuprate oxide. From the fact that the cuprate oxides are highly anisotropic systems, we study two cases of the junction barrier configurations, that is, the junctions with an insulating barrier parallel to the oxide layers and with the barrier perpendicular to the layers. In both cases we take the coordinates (x_1,x_2,x_3) in such a way that the x_1 and x_2 axes are parallel to the two principal axes on the junction barrier and the x_3 axis is perpendicular to the junction barrier. The position of the barrier is at $x_3=0$.

The superconducting current density inside the superconductors contacting the junction barrier is assumed to be described by the following anisotropic London equation:

$$\mathbf{J}(\mathbf{r},t)=-\frac{c}{4\pi}\hat{\lambda}^{-2}\left[\mathbf{A}(\mathbf{r},t)-\frac{\phi_0}{2\pi}\nabla\varphi(\mathbf{r},t)\right], \tag{4.1}$$

where $\varphi(\mathbf{r},t)$ is the phase of the superconducting order parameter and $\hat{\lambda}$ is the London penetration depth, which is, in the present system, a tensor defined by

$$\hat{\lambda}^{-2}=\begin{bmatrix}\lambda_1^{-2} & 0 & 0\\ 0 & \lambda_2^{-2} & 0\\ 0 & 0 & \lambda_3^{-2}\end{bmatrix}. \tag{4.2}$$

Assuming the uniaxial symmetry we take $\lambda_1=\lambda_2\equiv\lambda_a$ and $\lambda_3\equiv\lambda_c$ in the case where the junction barrier is parallel to the oxide layers, and $\lambda_1\equiv\lambda_c$ and $\lambda_2=\lambda_3\equiv\lambda_a$ in the other case where the barrier is perpendicular to the layers.

For the charge density $\rho(\mathbf{r},t)$ we assume the following form[49]

$$\rho(\mathbf{r},t)=-\frac{1}{4\pi\mu^2}\left[A_0(\mathbf{r},t)+\frac{\phi_0}{2\pi}\frac{1}{c}\frac{\partial}{\partial t}\varphi(\mathbf{r},t)\right], \tag{4.3}$$

where $A_0(\mathbf{r},t)$ is the scalar potential and μ is a constant of the order of the Thomas-Fermi screening length. The phase $\varphi(\mathbf{r},t)$ has a discontinuity at the junction-barrier site when a magnetic field or an electric field is present around the barrier site. As shown in Appendix B,[49,50] this discontinuity is described by the following conditions imposed upon the differential operations on $\varphi(\mathbf{r},t)$:

$$\left[\frac{\partial}{\partial x_3},\frac{\partial}{\partial x_1}\right]\varphi(\mathbf{r},t)=\frac{\partial}{\partial x_1}\chi(x_1,t)\delta(x_3), \tag{4.4}$$

$$\left[\frac{\partial}{\partial x_3},\frac{\partial}{\partial t}\right]\varphi(\mathbf{r},t)=\frac{\partial}{\partial t}\chi(x_1,t)\delta(x_3), \tag{4.5}$$

where $[A,B]=AB-BA$ and $\chi(x_1,t)$ is the phase difference at the junction barrier,

$$\chi(x_1,t)\equiv\varphi(x_1,x_3=+0,t)-\varphi(x_1,x_3=-0,t). \tag{4.6}$$

Substituting Eqs. (4.1) and (4.3) into the Maxwell equations and using Eqs. (4.4) and (4.5), we can derive the following equations for $\mathbf{H}=[0,H_2(x_1,x_3,t),0]$ and $\mathbf{E}=[E_1(x_1,x_3,t),0,E_3(x_1,x_3,t)]$,

$$\left[\frac{\epsilon_3}{c^2}\frac{\partial^2}{\partial t^2}-\left[\frac{\partial^2}{\partial x_1^2}+\zeta\frac{\partial^2}{\partial x_3^2}\right]+\lambda_3^{-2}\right]H_2(x_1,x_2,t)$$
$$=\frac{\phi_0}{2\pi\lambda_3^2}\frac{\partial}{\partial x_1}\chi(x_1,t)\delta(x_3)$$
$$+(\zeta\epsilon_1-\epsilon_3)\frac{1}{c}\frac{\partial^2}{\partial t\partial x_3}E_1(x_1,x_3,t), \tag{4.7}$$

$$\left[\frac{\epsilon_1}{c^2}\frac{\partial^2}{\partial t^2}-\left[\frac{\partial^2}{\partial x_1^2}+\frac{\partial^2}{\partial x_3^2}\right]+\lambda_1^{-2}\right]E_1(x_1,x_3,t)$$
$$+\frac{\partial}{\partial x_1}\left[\nabla\cdot\mathbf{E}-\frac{\mu^2}{\lambda_1^2}\nabla\cdot\hat{\epsilon}\mathbf{E}\right]=0, \tag{4.8}$$

$$\left[\frac{\epsilon_3}{c^2}\frac{\partial^2}{\partial t^2}-\left[\frac{\partial^2}{\partial x_1^2}+\frac{\partial^2}{\partial x_3^2}\right]+\lambda_3^{-2}\right]E_3(x_1,x_3,t)$$
$$+\frac{\partial}{\partial x_3}\left[\nabla\cdot\mathbf{E}-\frac{\mu^2}{\lambda_3^2}\nabla\cdot\hat{\epsilon}\mathbf{E}\right]$$
$$=\frac{\phi_0}{2\pi\lambda_3^2}\frac{1}{c}\frac{\partial}{\partial t}\chi(x_1,t)\delta(x_3), \tag{4.9}$$

where

$$\zeta=\lambda_1^2/\lambda_3^2, \tag{4.10}$$

and $\hat{\epsilon}$ is the dielectric tensor

$$\hat{\epsilon}=\begin{bmatrix}\epsilon_1 & 0 & 0\\ 0 & \epsilon_2 & 0\\ 0 & 0 & \epsilon_3\end{bmatrix}. \tag{4.11}$$

The relations $\epsilon_1=\epsilon_2\equiv\epsilon_a$ and $\epsilon_3\equiv\epsilon_c$ in the case of the barrier parallel to the oxide layers, and $\epsilon_1\equiv\epsilon_c$ and $\epsilon_2=\epsilon_3\equiv\epsilon_a$ in the other case are assumed.

Equations (4.7)–(4.9) are solved in terms of the phase difference $\chi(x_1,t)$ as

$$H_2(x_1,x_3,t)=\frac{\phi_0}{4\pi\lambda_3^2}\frac{1}{\sqrt{\zeta}}\int\frac{d\omega}{2\pi}\int\frac{dk_1}{2\pi}\frac{\Gamma_1(k_1,\omega)}{\sqrt{Z(k_1,\omega)}}\exp[-\sqrt{Z(k_1,\omega)/\zeta}|x_3|]\exp[ik_1x_1+i\omega t]$$
$$+\frac{\phi_0}{4\pi\mu^2}(\zeta\epsilon_1-\epsilon_3)\left[\frac{1}{\epsilon_3}-\frac{\mu^2}{\lambda_1^2}\right]\int\frac{d\omega}{2\pi}\int\frac{dk_1}{2\pi}\left[\frac{\omega}{c}\right]k_1\Gamma_t(k_1,\omega)$$

$$\times\left\{\frac{1}{\zeta}\frac{\sqrt{Z(k_1,\omega)/\zeta}\exp[-\sqrt{Z(k_1,\omega)/\zeta}|x_3|]}{[A^{(+)}(k_1,\omega)-Z(k_1,\omega)/\zeta][A^{(-)}(k_1,\omega)-Z(k_1,\omega)/\zeta]}\right.$$
$$+\frac{1}{\zeta}\frac{\sqrt{A^{(+)}(k_1,\omega)}\exp[-\sqrt{A^{(+)}(k_1,\omega)}|x_3|]}{[A^{(+)}(k_1,\omega)-A^{(-)}(k_1,\omega)][A^{(+)}(k_1,\omega)-Z(k_1,\omega)/\zeta]}$$
$$\left.-\frac{1}{\zeta}\frac{\sqrt{A^{(-)}(k_1,\omega)}\exp[-\sqrt{A^{(-)}(k_1,\omega)}|x_3|]}{[A^{(+)}(k_1,\omega)-A^{(-)}(k_1,\omega)][A^{(-)}(k_1,\omega)-Z(k_1,\omega)/\zeta]}\right\}\exp[ik_1x_1+i\omega t]\,, \tag{4.12}$$

$$E_1(x_1,x_3,t)=\frac{\phi_0}{4\pi\mu^2}\left[\frac{1}{\epsilon_3}-\frac{\mu^2}{\lambda_1^2}\right]\int\frac{d\omega}{2\pi}\int 3\frac{dk_1}{2\pi}\frac{-ik_1\Gamma_t(k_1,\omega)}{A^{(+)}(k_1,\omega)-A^{(-)}(k_1,\omega)}$$
$$\times\left\{\exp[-\sqrt{A^{(+)}(k_1,\omega)}|x_3|]-\exp[-\sqrt{A^{(-)}(k_1,\omega)}|x_3|]\right\}\exp[ik_1x_1+i\omega t]\,, \tag{4.13}$$

$$E_3(x_1,x_3,t)=\frac{\phi_0}{4\pi\mu^2}\left[\frac{\epsilon_1}{\epsilon_3}\right]\left[\frac{1}{\epsilon_1}-\frac{\mu^2}{\lambda_3^2}\right]\int\frac{d\omega}{2\pi}\int\frac{dk_1}{2\pi}\Gamma_t(k_1,\omega)$$
$$\times\left\{\frac{[A^{(+)}(k_1,\omega)-Y(k_1,\omega)]\sqrt{A^{(+)}(k_1,\omega)}\exp[-\sqrt{A^{(+)}(k_1,\omega)}|x_3|]}{[A^{(+)}(k_1,\omega)-A^{(-)}(k_1,\omega)][A^{(+)}(k_1,\omega)-(\epsilon_1/\epsilon_3)Z(k_1,\omega)]}\right.$$
$$\left.-\frac{[A^{(-)}(k_1,\omega)-Y(k_1,\omega)]\sqrt{A^{(-)}(k_1,\omega)}\exp[-\sqrt{A^{(-)}(k_1,\omega)}|x_3|]}{[A^{(+)}(k_1,\omega)-A^{(-)}(k_1,\omega)][A^{(-)}(k_1,\omega)-(\epsilon_1/\epsilon_3)Z(k_1,\omega)]}\right\}\exp[ik_1x_1+i\omega t]\,, \tag{4.14}$$

where

$$A^{(\pm)}(k_1,\omega)=\frac{1}{2}\left[Y(k_1,\omega)+\frac{\lambda_3^2}{\epsilon_3\mu^2}Z(k_1,\omega)-\frac{\lambda_3^2}{\mu^2}\left[\frac{1}{\epsilon_3}-\frac{\mu^2}{\lambda_1^2}\right]k_1^2\right]$$
$$\pm\frac{1}{2}\left\{\left[Y(k_1,\omega)+\frac{\lambda_3^2}{\epsilon_3\mu^2}Z(k_1,\omega)-\frac{\lambda_3^2}{\mu^2}\left[\frac{1}{\epsilon_3}-\frac{\mu^2}{\lambda_1^2}\right]k_1^2\right]^2\right.$$
$$\left.-4\left[\frac{\epsilon_1}{\epsilon_3}\right]\left[\frac{\lambda_3^2}{\epsilon_1\mu^2}Y(k_1,\omega)-\frac{\lambda_3^2}{\mu^2}\left[\frac{1}{\epsilon_3}-\frac{\mu^2}{\lambda_1^2}\right]k_1^2\right]Z(k_1,\omega)\right\}^{1/2}, \tag{4.15}$$

$$Y(k_1,\omega)=\frac{\epsilon_1}{\epsilon_3}k_1^2+\lambda_1^{-2}-\epsilon_1\frac{\omega^2}{c^2}+i0^+\,\mathrm{sgn}(\omega)\,, \tag{4.16}$$

$$Z(k_1,\omega)=k_1^2+\lambda_3^{-2}-\epsilon_3\frac{\omega^2}{c^2}+i0^+\,\mathrm{sgn}(\omega)\,. \tag{4.17}$$

The quantities $\Gamma_1(k_1,\omega)$ and $\Gamma_t(k_1,\omega)$ in Eqs. (4.12)–(4.14) are the Fourier transformations of the derivatives of the phase difference

$$\Gamma_1(k_1,\omega)=\int dx_1dt\frac{\partial}{\partial x_1}\chi(x_1,t)\exp(-ik_1x_1-i\omega t)\,, \tag{4.18}$$

$$\Gamma_t(k_1,\omega)=\int dx_1dt\frac{1}{c}\frac{\partial}{\partial t}\chi(x_1,t)\exp(-ik_1x_1-i\omega t)\,. \tag{4.19}$$

In Eqs. (4.16) and (4.17) we added an infinitesimal imaginary part $i0^+\mathrm{sgn}(\omega)$ to ensure the causality.[51] It is noted that

the electromagnetic fields given in Eqs. (4.12)–(4.14) include the contribution from the induced charge around the junction barrier

$$\rho(x_1,x_3,t)=-\frac{\phi_0}{16\pi^2\mu^2}\int\frac{d\omega}{2\pi}\int\frac{dk_1}{2\pi}\frac{\Gamma_t(k_1,\omega)}{A^{(+)}(k_1,\omega)-A^{(-)}(k_1,\omega)}$$
$$\times\left\{[A^{(+)}(k_1,\omega)-Y(k_1,\omega)]\exp[-\sqrt{A^{(+)}(k_1,\omega)}|x_3|]\right.$$
$$\left.-[A^{(-)}(k_1,\omega)-Y(k_1,\omega)]\exp[-\sqrt{A^{(-)}(k_1,\omega)}|x_3|]\right\}\exp[ik_1x_1+i\omega t]\ . \tag{4.20}$$

From Eqs. (4.12)–(4.14) we can calculate the current passing through the junction barrier using the Maxwell equation

$$\partial H_2(x_1,0,t)/\partial x_1=4\pi J_3(x_1,0,t)/c$$
$$+(\epsilon_3/c)\partial E_3(x_1,0,t)/\partial t\ .$$

We assume that the total current flowing inside the barrier is the tunneling current which is given by a sum of the Josephson current, the single-particle current, and the displacement current. Then from the condition of continuation of the total current we require the following relation:[52,53]

$$\frac{c}{4\pi}\frac{\partial}{\partial x_1}H_2(x_1,0,t)=J_c\sin\chi(x_1,t)+\frac{1}{R}V(x_1,t)$$
$$+C\frac{\partial}{\partial t}V(x_1,t)\ , \tag{4.21}$$

where $V(x_1,t)$ is the voltage across the junction and R and C are, respectively, the resistance and capacitance of the junction per unit area. Substitution of Eq. (4.12) into Eq. (4.21) leads to the following equation for the phase difference $\chi(x_1,t)$:

$$\int dx_1'dt'K(x_1-x_1',t-t')\frac{\partial^2}{\partial x_1'^2}\chi(x_1',t')$$
$$=\frac{16\pi^2\lambda_1}{\phi_0 c}\left[J_c\sin\chi(x_1,t)+\frac{1}{R}V(x_1,t)\right.$$
$$\left.+C\frac{\partial}{\partial t}V(x_1,t)\right]\ , \tag{4.22}$$

where $K(x_1,t)$ is a function defined through the following Fourier transformation:

$$K(k_1,\omega)=\frac{(\lambda_1/\lambda_3^2)}{Z(k_1,\omega)}$$
$$\times\frac{\sqrt{A^{(+)}(k_1,\omega)}\sqrt{A^{(-)}(k_1,\omega)}+Z(k_1,\omega)/\zeta}{\sqrt{A^{(+)}(k_1,\omega)}+\sqrt{A^{(-)}(k_1,\omega)}}\ . \tag{4.23}$$

The isotropic limit of Eq. (4.23) is calculated as

$$K(k_1,\omega)\to\frac{1}{\sqrt{\lambda^2k_1^2+1-\epsilon\lambda^2\omega^2/c^2}}\ . \tag{4.24}$$

Let us now solve Eq. (4.22). First we consider the case where the single-particle current can be neglected ($R\to\infty$). As a solution of Eq. (4.22) we seek the solution of the form

$$\chi(x_1,t)=qx_1+\omega_0t+\theta(x_1,t)\ , \tag{4.25}$$

where $\theta(x_1,t)$ is assumed to be a Fourier-transformable function. The constants q and ω_0 in Eq. (4.25) are determined later. Under the assumption

$$V(x_1,t)=(\hbar/2e)\partial\chi(x_1,t)/\partial t\ , \tag{4.26}$$

Eq. (4.22) is reduced in the linear approximation to

$$\int dx_1'dt'K(x_1-x_1',t-t')\frac{\partial^2}{\partial x_1'^2}\theta(x_1',t')-\frac{1}{\bar{c}^2}\frac{\partial^2}{\partial t^2}\theta(x_1,t)$$
$$=\frac{16\pi^2\lambda_1}{\phi_0 c}J_c\sin(qx_1+\omega_0t)\ , \tag{4.27}$$

where $\bar{c}$ is defined as

$$\bar{c}=\frac{c}{\sqrt{8\pi\lambda_1 C}}\ . \tag{4.28}$$

This equation is easily solved as

$$\theta(x_1,t)=\frac{1}{\lambda_J^2}\,\mathrm{Im}\left[\frac{\exp[iqx_1+i\omega_0t]}{-q^2K(q,\omega_0)+(\omega_0^2/\bar{c}^2)}\right]\ , \tag{4.29}$$

where

$$\lambda_J=\left[\frac{\hbar c^2}{16\pi e\lambda_1 J_c}\right]^{1/2}\ . \tag{4.30}$$

As noted from Eqs. (4.23), $K(q,\omega_0)$ is complex when $A^{(\pm)}(q,\omega_0)<0$. Substituting Eq. (4.29) into Eq. (4.25) and noting Eqs. (4.18) and (4.19), we can rewrite Eqs. (4.12)–(4.14) in the following form:

$$H_2(x_1,x_3,t)=H_{dc}(x_3)+\frac{\phi_0}{4\pi\mu^2}\frac{1}{\lambda_J^2}(\zeta\epsilon_1-\epsilon_3)\left[\frac{1}{\epsilon_3}-\frac{\mu^2}{\lambda_1^2}\right]$$
$$\times\mathrm{Re}\left[\frac{q(\omega_0^2/c^2)\exp(iqx_1+i\omega_0 t)}{[-q^2K(q,\omega_0)+(\omega_0^2/\bar{c}^2)][A^{(+)}(q,\omega_0)-A^{(-)}(q,\omega_0)]}\right.$$
$$\times\left\{\frac{\sqrt{A^{(+)}(q,\omega_0)}}{\zeta A^{(+)}(q,\omega_0)-Z(q,\omega_0)}\exp(-\sqrt{A^{(+)}(q,\omega_0)}|x_3|)\right.$$
$$\left.\left.-\frac{\sqrt{A^{(-)}(q,\omega_0)}}{\zeta A^{(-)}(q,\omega_0)-Z(q,\omega_0)}\exp(-\sqrt{A^{(-)}(q,\omega_0)}|x_3|)\right\}\right], \tag{4.31}$$

$$E_1(x_1,x_3,t)=\frac{\phi_0}{4\pi\mu^2}\frac{1}{\lambda_J^2}\left[\frac{1}{\epsilon_3}-\frac{\mu^2}{\lambda_1^2}\right]$$
$$\times\mathrm{Re}\left[\frac{-iq(\omega_0/c)\exp(iqx+i\omega_0 t)}{[-q^2K(q,\omega_0)+(\omega_0^2/\bar{c}^2)][A^{(+)}(q,\omega_0)-A^{(-)}(q,\omega_0)]}\right.$$
$$\left.\times\left\{\exp[-\sqrt{A^{(+)}(q,\omega_0)}|x_3|]-\exp[-\sqrt{A^{(-)}(q,\omega_0)}|x_3|]\right\}\right], \tag{4.32}$$

$$E_3(x_1,x_3,t)=E_{dc}(x_3)+\frac{\phi_0}{4\pi\mu^2}\frac{1}{\lambda_J^2}\left[\frac{\epsilon_1}{\epsilon_3}\right]\left[\frac{1}{\epsilon_1}-\frac{\mu^2}{\lambda_3^2}\right]$$
$$\times\mathrm{Re}\left[\frac{(\omega_0/c)\exp(iqx_1+i\omega_0 t)}{[-q^2K(q,\omega_0)+(\omega_0^2/\bar{c}^2)][A^{(+)}(q,\omega_0)-A^{(-)}(q,\omega_0)]}\right.$$
$$\times\left\{\frac{[A^{(+)}(q,\omega_0)-Y(q,\omega_0)]\sqrt{A^{(+)}(q,\omega_0)}}{A^{(+)}(q,\omega_0)-(\epsilon_1/\epsilon_3)Z(q,\omega_0)}\exp[-\sqrt{A^{(+)}(q,\omega_0)}|x_3|]\right.$$
$$\left.\left.-\frac{[A^{(-)}(q,\omega_0)-Y(q,\omega_0)]\sqrt{A^{(-)}(q,\omega_0)}}{A^{(-)}(q,\omega_0)-(\epsilon_1/\epsilon_3)Z(q,\omega_0)}\exp[-\sqrt{A^{(-)}(q,\omega_0)}|x_3|]\right\}\right], \tag{4.33}$$

where $H_{dc}(x_3)$ and $E_{dc}(x_3)$ are the dc parts of the electromagnetic fields

$$H_{dc}(x_3)=\frac{\phi_0 q}{4\pi\lambda_1}\exp(-|x_3|/\lambda_1), \tag{4.34}$$

$$E_{dc}(x_3)=\frac{\phi_0}{4\pi\sqrt{\epsilon_3\mu}}\left[\frac{\omega_0}{c}\right]\exp\left[-\frac{|x_3|}{\sqrt{\epsilon_3\mu}}\right]. \tag{4.35}$$

The dc parts originate from the delta functions $\delta(k_1)\delta(\omega)$ in $\Gamma_1(k_1,\omega)$ and $\Gamma_t(k_1,\omega)$ as seen from Eqs. (4.18), (4.19), and (4.25). From the assumptions, $H_{dc}(0)=H_{ex}$ and $\int_{-\infty}^{\infty}dz\,E_{dc}(x_3)=V_0$, we can relate the constants, q and ω_0, respectively, to the external magnetic field H_{ex} and the voltage across the junction V_0 as

$$q=\frac{4\pi\lambda_1}{\phi_0}H_{ex}, \tag{4.36}$$

$$\omega_0=\frac{2e}{\hbar}V_0. \tag{4.37}$$

The dc magnetic field and the dc electric field can penetrate into the superconductors within the distances, respectively, λ_1 and $\sqrt{\epsilon_3\mu}$ along the x_3 axis ($\lambda_1\gg\sqrt{\epsilon_3\mu}$). On the other hand, as seen in Eqs. (4.31)–(4.33), the penetration depth of the ac part of the electromagnetic field along the x_3 axis is given by $1/\sqrt{A^{(\pm)}(q,\omega)}$, and therefore it is dependent on the applied magnetic field and the voltage. When $A^{(\pm)}(q,\omega)>0$, the ac field is confined around the junction barrier as well as the dc field. As shown in the following, $A^{(\pm)}(q,\omega)$ can be negative in some region of (q,ω). In this region the ac field changes to a propaga-

ting wave with a propagation vector having the x_3 component along with the x_1 component.

A. Polynting vector of excited plasma

Let us now study the behavior of the ac parts of the electric and magnetic fields. In the following we consider the cases of two different configurations of the junction barrier.

1. *Barrier ∥ oxide layers*

In this configuration the penetration depth and dielectric constant are, respectively, given by $\lambda_1=\lambda_a,\lambda_3=\lambda_c$, and $\epsilon_1=\epsilon_1,\epsilon_3=\epsilon_c$. The plasma frequencies expressed by $\omega_i=c/(\lambda_i\sqrt{\epsilon_i})$ are given by $\omega_1=\omega_{pa}$ and $\omega_3=\omega_{pc}$. Noting the fact that $\sqrt{\epsilon_a\mu}\ll\lambda_a,\lambda_c$, we may approximate the ac part of the magnetic and electric fields Eqs. (4.31)–(4.33) in the strong anisotropic limit ($\omega_{pc}\ll\omega_{pa}$) as follows:

$$H_2^{\rm ac}(x_1,x_3,t)\simeq\frac{\phi_0}{4\pi\lambda_J^2}\,{\rm Re}\left[\left\{\frac{(q/\lambda_a^2)\sqrt{\lambda_c^2q^2+1-(\omega_0^2/\omega_{pc}^2)}}{-q^2+(\omega_0^2/\bar{c}^2)\sqrt{[\lambda_c^2q^2+1-(\omega_0^2/\omega_{pc}^2)]}\sqrt{[1-(\omega_0^2/\omega_{pc}^2)]}}\right.\right.$$
$$\times\sqrt{\epsilon_c\mu}\,\frac{(\omega_0^2/\omega_{pc}^2)}{(\omega_0^2/\omega_{pc}^2)-1}\exp\left[-\sqrt{1-\omega_0^2/\omega_{pc}^2}\,\frac{|x_3|}{\sqrt{\epsilon_c\mu}}\right]$$
$$+\frac{(\lambda_c^2/\lambda_a)q}{-q^2+(\omega_0^2/\bar{c}^2)\sqrt{[\lambda_c^2q^2+1-(\omega_0^2/\omega_{pc}^2)]}\sqrt{[1-(\omega_0^2/\omega_{pc}^2)]}}$$
$$\left.\left.\times\exp\left[-\sqrt{[\lambda_c^2q^2+1-(\omega_0^2/\omega_{pc}^2)]/[1-(\omega_0^2/\omega_{pc}^2)]}\,\frac{|x_3|}{\lambda_a}\right]\right\}\exp(iqx_1+i\omega_0t)\right],\qquad(4.38)$$

$$E_1^{\rm ac}(x_1,x_3,t)\simeq\frac{\phi_0}{4\pi\lambda_J^2}\,{\rm Re}\left[\frac{-iq(\omega_0/c)\sqrt{\lambda_c^2q^2+1-(\omega_0^2/\omega_{pc}^2)}/\sqrt{1-(\omega_0^2/\omega_{pc}^2)}}{-q^2+(\omega_0^2/\bar{c}^2)\sqrt{[\lambda_c^2q^2+1-(\omega_0^2/\omega_{pc}^2)]}\sqrt{[1-(\omega_0^2/\omega_{pc}^2)]}}\right.$$
$$\times\left\{\exp\left[-\sqrt{1-\omega_0^2/\omega_{pc}^2}\cdot\frac{|x_3|}{\sqrt{\epsilon_c\mu}}\right]\right.$$
$$\left.\left.-\exp\left[-\sqrt{[\lambda_c^2q^2+1-(\omega_0^2/\omega_{pc}^2)]/[1-(\omega_0^2/\omega_{pc}^2)]}\,\frac{|x_3|}{\lambda_a}\right]\right\}\exp(iqx_1+i\omega_0t)\right],\qquad(4.39)$$

$$E_3^{\rm ac}(x_1,x_3,t)\simeq\frac{\phi_0}{4\pi\lambda_J^2}\,{\rm Re}\left[\left\{\frac{(\omega_0/c)\sqrt{\lambda_c^2q^2+1-(\omega_0^2/\omega_{pc}^2)}}{-q^2+(\omega_0^2/\bar{c}^2)\sqrt{[\lambda_c^2q^2+1-(\omega_0^2/\omega_{pc}^2)]}\sqrt{[1-(\omega_0^2/\omega_{pc}^2)]}}\right.\right.$$
$$\times\frac{1}{\sqrt{\epsilon_c\mu}}\exp\left[-\sqrt{1-\omega_0^2/\omega_{pc}^2}\,\frac{|x_3|}{\sqrt{\epsilon_c\mu}}\right]$$
$$-\frac{(\omega_0/c)\lambda_a^{-1}(\lambda_cq)^2}{-q^2+(\omega_0^2/\bar{c}^2)\sqrt{[\lambda_c^2q^2+1-(\omega_0^2/\omega_{pc}^2)]}\sqrt{[1-(\omega_0^2/\omega_{pc}^2)]}}\,\frac{1}{1-(\omega_0^2/\omega_{pc}^2)}$$
$$\left.\left.\times\exp\left[-\sqrt{[\lambda_c^2q^2+1-(\omega_0^2/\omega_{pc}^2)]/[1-(\omega_0^2/\omega_{pc}^2)]}\,\frac{|x_3|}{\lambda_a}\right]\right\}\exp(iqx_1+i\omega_0t)\right].\qquad(4.40)$$

In this configuration the ac fields have two components with different spatial dependence along the x_3 direction ($\|c$ axis), i.e.,

$$\exp\left[-\sqrt{1-\omega_0^2/\omega_{pc}^2}\,\frac{|x_3|}{\sqrt{\epsilon_c\mu}}\right]$$

and

$$\exp\left[-\sqrt{[\lambda_c^2q^2+1-(\omega_0^2/\omega_{pc}^2)]/[1-(\omega_0^2/\omega_{pc}^2)]}\,\frac{|x_3|}{\lambda_a}\right].$$

These two exponential functions change from decay functions to plane-wave functions in the frequency regions, respectively, $\omega_{pc}<\omega_0$ and $\omega_{pc}<\omega_0<\omega_T(q)\equiv\omega_{pc}\sqrt{\lambda_c^2q^2+1}$. In these regions the electric and magnet-

ic fields propagate inside the superconductors because the propagation vectors have the components perpendicular to the junction barrier. Therefore, the ac Josephson current can excite the bulk plasma mode in these frequency regions. At a frequency in the region $\omega_{pc}<\omega_0<\omega_T(q)$ two bulk plasma modes with different wave numbers,

$$\mathbf{k}^{(1)}=\left[q,-\frac{1}{\sqrt{\epsilon_c\mu}}\sqrt{\omega_0^2/\omega_{pc}^2-1}\right]$$

and

$$\mathbf{k}^{(2)}=\left[q,-\frac{1}{\lambda_a}\sqrt{[\lambda_c^2q^2+1-(\omega_0^2/\omega_{pc}^2)]/[(\omega_0^2/\omega_{pc}^2)-1]}\right]$$

are excited. The latter plasma mode with $\mathbf{k}^{(2)}$ is again quenched above the frequency $\omega_T(q)$. In Fig. 6 we plot the time average of the Poynting vector $S_1\equiv(c/4\pi)(\mathbf{E}^{ac}\times\mathbf{H}^{ac})_1$ as a function of the frequency for the parameter values $\lambda_c=2\times10^{-4}$ cm, $\lambda_a=2\times10^{-5}$ cm, $\epsilon_c=25$, and $\bar{c}/c=0.05$. The time average of the Poynting vector along the direction perpendicular to the junction barrier, $S_3\equiv(c/4\pi)$ $(\mathbf{E}^{ac}\times\mathbf{H}^{ac})_3$, is very small, so that the energy of the electromagnetic field flows along the direction parallel to the junction barrier in this configuration. It is noted that the direction of the Poynting vector is different from the propagation direction of the electromagnetic phase wave. As seen in Fig. 6, S_1 has two peaks at frequencies near ω_{pc} and $\omega_T(q)$. These peaks originate from the resonance with the bulk plasma modes with the wave numbers $\mathbf{k}^{(1)}$ and $\mathbf{k}^{(2)}$. The peak situated at the higher frequency is sensitive to the applied magnetic field as seen in Fig. 6. Since these plasma waves decay into electromagnetic waves, the radiation of the electromagnetic waves from the direction parallel to the junction barrier will be expected in the narrow regions of the applied voltage near $V_0\sim\hbar\omega_{pc}/2e$ and $V_0\sim\hbar\omega_T(q)/2e$. As seen in Fig. 6, the magnitude of the Poynting vector diverges at ω_{pc}. The divergence comes from zero plasma damping which we assume. Actually there is some weak plasma damping which suppresses the divergence. If we take 10^4 for $S_1/[(c/8\pi)(\phi_0/4\pi\lambda_J^2)^2]$, the power of the emitted electromagnetic wave is in the range of 0.03–300 W/cm^2 for the λ_J value of 10^{-2}–10^{-3} cm.

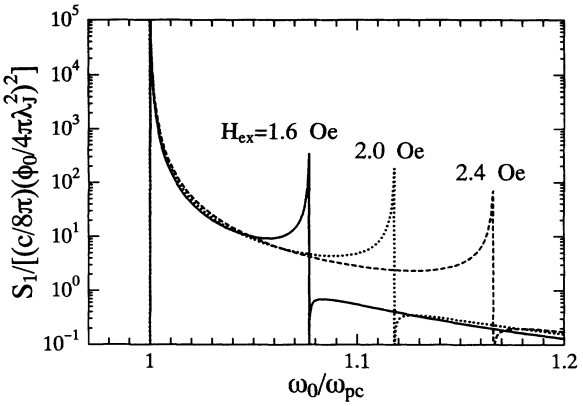

FIG. 6. Time average of the Poynting vector of the plasma generated in a Josephson junction with the barrier parallel to the oxide layers. The time average of the Poynting vector parallel to the barrier, S_1, is plotted as a function of Josephson frequency ω_0 for three magnetic fields. The time average of the Poynting vector and the Josephson frequency are normalized by $(c/8\pi)(\phi_0/4\pi\lambda_J^2)^2$ and ω_{pc}, respectively.

2. *Barrier ⊥ oxide layers*

In this configuration the penetration depth and the dielectric constant are given by $\lambda_1=\lambda_c,\lambda_3=\lambda_a$, and $\epsilon_1=\epsilon_c,\epsilon_3=\epsilon_a$, so that the plasma frequencies are reduced to $\omega_{p1}=\omega_{pc}$ and $\omega_{p3}=\omega_{pa}$. Using the same approximation as in Sec. IV A 1, we obtain the magnetic and electric fields from Eqs. (4.31)–(4.33) as follows:

$$H_2^{ac}(x_1,x_3,t)\simeq\frac{\phi_0}{4\pi\lambda_J^2}\,\mathrm{Re}\left[\frac{(q/\lambda_c)\sqrt{[1-(\omega_0^2/\omega_{pc}^2)]/[1+\lambda_a^2q^2]}}{-q^2\sqrt{[1-(\omega_0^2/\omega_{pc}^2)]/[1+\lambda_a^2q^2]}+(\omega_0^2/\bar{c}^2)}\right.$$
$$\left.\times\exp\left[-\sqrt{[1-\omega_0^2/\omega_{pc}^2][1+\lambda_a^2q^2]}\frac{|x_3|}{\lambda_c}\right]\exp(iqx_1+i\omega_0t)\right],\tag{4.41}$$

$$E_1^{ac}(x_1,x_3,t)\simeq\frac{\phi_0}{4\pi\lambda_J^2}\,\mathrm{Re}\left[\frac{iq(\omega_0/c)}{-q^2\sqrt{[1-(\omega_0^2/\omega_{pc}^2)]/[1+\lambda_a^2q^2]}+(\omega_0^2/\bar{c}^2)}\right.$$
$$\left.\times\exp\left[-\sqrt{[1-\omega_0^2/\omega_{pc}^2][1+\lambda_a^2q^2]}\frac{|x_3|}{\lambda_c}\right]\exp(iqx_1+i\omega_0t)\right],\tag{4.42}$$

$$E_3^{ac}(x_1,x_3,t)\simeq\frac{\phi_0}{4\pi\lambda_J^2}\,\mathrm{Re}\left[\frac{\lambda_a^2}{\lambda_c^2}\frac{\lambda_cq^2(\omega_0/c)\sqrt{[1-(\omega_0^2/\omega_{pc}^2)]/[1+\lambda_a^2q^2]}}{-q^2\sqrt{[1-(\omega_0^2/\omega_{pc}^2)]/[1+\lambda_a^2q^2]}+(\omega_0^2/\bar{c}^2)}\right.$$
$$\left.\times\exp\left[-\sqrt{[1-\omega_0^2/\omega_{pc}^2][1+\lambda_a^2q^2]}\frac{|x_3|}{\lambda_c}\right]\exp(iqx_1+i\omega_0t)\right].\tag{4.43}$$

It is noted that the ac electric field is almost parallel to the junction barrier ($|E_1^{ac}| \gg |E_3^{ac}|$), since $\lambda_a^2/\lambda_c^2 \ll 1$ in the present strong anisotropic system. This result is sharply contrasted with that in the previous configuration.

As seen in Eqs. (4.41)–(4.43), the ac electromagnetic field changes to a propagating wave above the plasma frequency ω_{pc}. The wave vector of the wave is given by

$$\mathbf{k} \equiv (k_1, k_3) = \{q, -(1/\lambda_c)\sqrt{[(\omega_0^2/\omega_{pc}^2)-1][1+\lambda_a^2 q^2]}\}$$

in the region $\omega_0 \geq \omega_{pc}$. In Fig. 7 the time average of the Poynting vector S_3 is plotted for the same parameter values as in the previous case. As seen in this figure, S_3 has a peak near the plasma frequency and vanishes at ω_{pc}. The reason for the Poynting vector vanishing is as follows. At $\omega_0 = \omega_{pc}$ the electric field propagates in the direction parallel to the junction barrier (i.e., $\mathbf{k} \parallel$ the c axis) and the magnetic field vanishes. The electromagnetic field is purely longitudinal at the frequency. As the frequency increases, the propagation direction gradually rotates and acquires a transverse component. Therefore, in the region

$$(1/\lambda_c)\sqrt{[(\omega_0^2/\omega_{pc}^2)-1][1+\lambda_a^2 q^2]} \gg q$$

the transverse bulk plasma propagating in the direction perpendicular to the junction barrier is excited. This plasma excitation will be detected by observing the emission of an electromagnetic wave propagating along the direction perpendicular to the junction barrier. It is noted that the direction of the emitted light is perpendicular to that of the Swihart mode.[55] When the Josephson penetration depth is assumed to be in the range of $\lambda_J = 10^{-3}$–10^{-4} cm, the power of the emitted light at the peak frequency for $H_{ex} = 12$ Oe in Fig. 7 is estimated to be 1.8×10^{-4}–1.8 W/cm^2. Since J_c in this junction configuration is expected to be larger than J_c in the configuration of Sec. IV A 1, we took smaller values of λ_J for this junction.

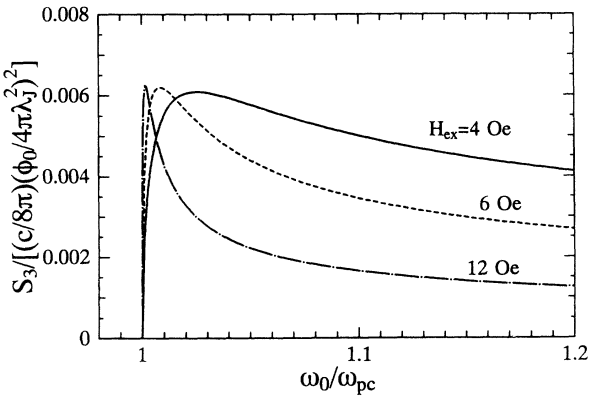

FIG. 7. Time average of the Poynting vector of the plasma generated in a Josephson junction with the barrier perpendicular to the oxide layers. The time average of the Poynting vector perpendicular to the barrier, S_3, is plotted as a function of Josephson frequency ω_0. The time average of the Poynting vector and the Josephson frequency are normalized by $(c/8\pi)(\phi_0/4\pi\lambda_J^2)^2$ and ω_{pc}, respectively.

B. *I-V* characteristics

Let us next investigate the effect of the low-frequency plasma on the *I-V* characteristics of the Josephson current. We assume the junction size along the x_1 axis to be much larger than $2\pi/q$. We consider the following linearized equation including the single-particle tunneling current for $\theta(x_1,t)$:

$$\int dx_1' dt' K(x_1 - x_1', t-t') \frac{\partial^2}{\partial x_1'^2}\theta(x_1',t') - \frac{1}{\bar{c}^2}\frac{\partial^2}{\partial t^2}\theta(x_1,t) - \frac{8\pi\lambda_a}{c^2 R}\frac{\partial}{\partial t}\theta(x_1,t) = \frac{1}{\lambda_J^2}\sin(qx_1+\omega_0 t) . \quad (4.44)$$

The solution is obtained as

$$\theta(x_1,t) = \frac{1}{\lambda_J^2}\,\mathrm{Im}\left[\frac{\exp[iqx_1+i\omega_0 t]}{-q^2K(q,\omega_0)+(\omega_0^2/\bar{c}^2)-iQ^{-1}(\omega_0^2/\bar{c}^2)}\right], \quad (4.45)$$

where

$$Q = \frac{R\omega_0 c^2}{8\pi\lambda_1\bar{c}^2} . \quad (4.46)$$

The dc Josephson current is calculated as

$$I_J = \lim_{T\to\infty, L\to\infty}\frac{1}{T}\int_0^\infty dt\frac{1}{L}\int_0^\infty dx_1 J_c \sin[qx_1+\omega_0 t+\theta(x_1,t)] \simeq \lim_{T\to\infty, L\to\infty}\frac{1}{T}\int_0^\infty dt\frac{1}{L}\int_0^\infty dx_1 J_c\cos(qx_1+\omega_0 t)\theta(x_1,t) . \quad (4.47)$$

Substituting Eq. (4.45) into Eq. (4.47), we find the dc Josephson current

$$I_J = J_c\frac{\bar{c}^2}{2\lambda_J^2\omega_0^2}\left[\frac{\bar{c}^2q^2}{\omega_0^2}K_2(q,\omega)+Q^{-1}\right]\left[\left[1-\frac{\bar{c}^2q^2}{\omega_0^2}K_1(q,\omega_0)\right]^2+\left[\frac{\bar{c}^2q^2}{\omega_0^2}K_2(q,\omega_0)+Q^{-1}\right]^2\right]^{-1}, \quad (4.48)$$

where $K_1(q,\omega_0)$ and $K_2(q,\omega_0)$ are, respectively, the real and imaginary parts of $K(q,\omega_0)$.

To simplify the problem we confine ourselves to the limiting case of $\mu/\lambda_{a,c} \to 0$ in the following. In this limit the

function $K(q,\omega)$ is reduced to

$$K(q,\omega_0)\sim\frac{\sqrt{1-(\omega_0^2/\omega_{p1}^2)}}{\sqrt{\lambda_3^2q^2+1-(\omega_0^2/\omega_{p3}^2)}\sqrt{1-(\omega_0^2/\omega_{p3}^2)}}\ . \tag{4.49}$$

1. *Barrier ∥ oxide layers*

Taking $\omega_{p1}=\omega_{pa}$ and $\omega_{p3}=\omega_{pc}$ in Eq. (4.46) and assuming $\omega_{pc}\ll\omega_{pa}$, we obtain the dc Josephson current in this case as

$$I_J=J_c\frac{\bar{c}^2}{2\lambda_J^2\omega_0^2}Q^{-1}\left[\left[1-\frac{(\bar{c}^2q^2/\omega_0^2)}{\sqrt{[\lambda_c^2q^2+1-(\omega_0^2/\omega_{pc}^2)][1-(\omega_0^2/\omega_{pc}^2)]}}\right]^2+Q^{-2}\right]^{-1}, \tag{4.50}$$

for $\omega_0<\omega_{pc}$ and $\omega_0>\omega_T(q)\equiv\omega_{pc}\sqrt{\lambda_c^2q^2+1}$, and

$$I_J=J_c\frac{\bar{c}^2}{2\lambda_J^2\omega_0^2}\left[-\frac{(\bar{c}^2q^2/\omega_0^2)}{\sqrt{[\lambda_c^2q^2+1-(\omega_0^2/\omega_{pc}^2)][(\omega_0^2/\omega_{pc}^2)-1]}}+Q^{-1}\right]$$
$$\times\left[1+\left[-\frac{(\bar{c}^2q^2/\omega_0^2)}{\sqrt{[\lambda_c^2q^2+1-(\omega_0^2/\omega_{pc}^2)][(\omega_0^2/\omega_{pc}^2)-1]}}+Q^{-1}\right]^2\right]^{-1}, \tag{4.51}$$

or $\omega_{pc}<\omega_0<\omega_T(q)$.

In Fig. 8 we show the *I-V* characteristics calculated from Eqs. (4.50) and (4.51). We used the parameter values of $Q/(\omega_0/\omega_{pc})=5$ and $\bar{c}/c=0.05$. As seen in this figure, the dc Josephson current has two peaks below the plasma voltage $\hbar\omega_{pc}/2e$. The positions of the two peaks are obtained from the solutions of the equation for ω_0,

$$\sqrt{[\lambda_c^2q^2+1-(\omega_0^2/\omega_{pc}^2)]}\sqrt{[1-(\omega_0^2/\omega_{pc}^2)]}=\frac{\bar{c}^2q^2}{\omega_0^2}\ . \tag{4.52}$$

This equation has two real solutions corresponding to the frequencies of an electromagnetic field propagating along the junction, which we call the junction wave from now on. The junction wave with a lower frequency has a dispersion $\omega_0\simeq\bar{c}q$ for $q\to0$. This mode corresponds to the Swihart mode in the conventional Josephson junction.[54] The larger peak of the dc current at a lower voltage originates from the resonance of the ac Josephson current with the Swihart mode.[55] Another real solution of Eq. (4.52) has a dispersion which starts from ω_{pc} at $q=0$ and decreases with increasing q. This junction wave is also surface mode localized near the barrier, which is analogous to the surface plasmon. The second peak in the *I-V* characteristics is caused by the resonance of the Josephson current with this junction mode. When V_0 is equal to the plasma voltage $\hbar\omega_{pc}/2e$ the dc Josephson current vanishes as seen in Fig. 9.

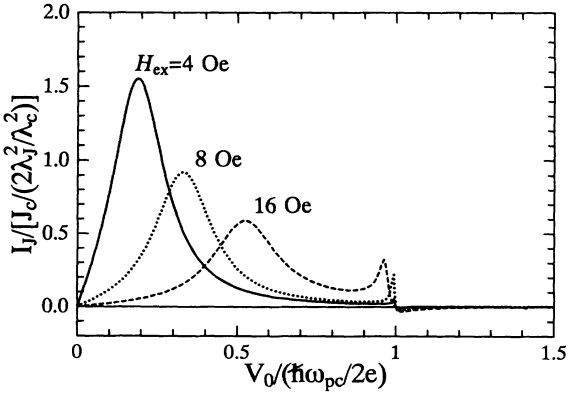

FIG. 8. *I-V* characteristics of a Josephson junction with the barrier parallel to the oxide layers. The dc Josephson current I_J is plotted as a function of applied voltage V_0 for the applied magnetic fields of $H_{ex}=4$, 8, and 16 Oe. The dc Josephson current and the applied voltage are normalized by $J_c/(2\lambda_J^2/\lambda_c^2)$ and $\hbar\omega_{pc}/(2e)$, respectively.

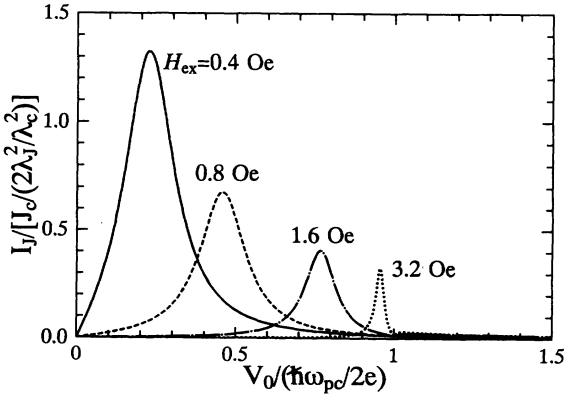

FIG. 9. *I-V* characteristics of a Josephson junction with the barrier perpendicular to the oxide layers. The dc Josephson current I_J is plotted as a function of applied voltage V_0 for the applied magnetic fields of $H_{ex}=0.4$, 0.8, 1.6, and 3.2 Oe. The dc Josephson current and the applied voltage are normalized by $J_c/(2\lambda_J^2/\lambda_c^2)$ and $\hbar\omega_{pc}/(2e)$, respectively.

In the region $\omega_{pc}<\omega_0<\omega_T(q)$ the Josephson current has a small negative value, that is, the current flows in the direction opposite to the applied voltage. However as shown in Appendix C, the total dc current across the junction, which is composed of the Josephson current, the single-electron current, and the displacement current, flows in the normal direction.

2. Barrier ⊥ oxide layers

In this configuration the plasma frequencies are $\omega_{p1}=\omega_{pc}$ and $\omega_{p3}=\omega_{pa}$. The *I-V* characteristics is derived in the strong anisotropic case ($\omega_{pc}\ll\omega_{pa}$) as follows:

$$I_J=J_c\frac{\bar{c}^2}{2\lambda_J^2\omega_0^2}Q^{-1}\left[\left[1-\frac{\bar{c}^2q^2}{\omega_0^2}\sqrt{(1-\omega_0^2/\omega_{pc}^2)/(1+\lambda_a^2q^2)}\right]^2+Q^{-2}\right]^{-1}, \tag{4.53}$$

for $\omega_0<\omega_{pc}$ and

$$I_J=J_c\frac{\bar{c}^2}{2\lambda_J^2\omega_0^2}\left[\frac{\bar{c}^2q^2}{\omega_0^2}\sqrt{(\omega_0^2/\omega_{pc}^2-1)/(1+\lambda_a^2q^2)}+Q^{-1}\right]\left[1+\left[\frac{\bar{c}^2q^2}{\omega_0^2}\sqrt{(\omega_0^2/\omega_{pc}^2-1)(1+\lambda_a^2q^2)}+Q^{-1}\right]^2\right]^{-1}, \tag{4.54}$$

for $\omega_0>\omega_{pc}$.

In Fig. 9 we plot I_J as a function of the applied voltage V_0 in the case of $Q/(\omega_0/\omega_{pc})=5$ and $\bar{c}/c=0.05$. The dc Josephson current takes a maximum value at a voltage satisfying the relation

$$\omega_0^2=\bar{c}^2q^2\sqrt{1-(\omega_0^2/\omega_{pc}^2)}\ . \tag{4.55}$$

This relation yields a solution $\omega_0\simeq\bar{c}q$ in the region $\omega_0\ll,\omega_{pc}$, which corresponds to the Swihart mode.[54] Thus the peak in the *I-V* characteristics arises from the resonance of the ac Josephson current with the Swihart mode.[55] As seen from Eq. (4.55), the Swihart mode is always below the plasma frequency ω_{pc}. The dc Josephson current does not show any anomaly at the plasma voltage, so that the *I-V* characteristics in this configuration is similar to that in conventional Josephson junctions.

V. SUMMARY

One of the striking properties of the cuprate superconductors is that the frequency of the plasma with *c*-axis polarization is extremely low.[1,2] Since the frequency is lower than the superconducting energy gap, the damping of the plasma is very weak. We predict that various electromagnetic phenomena arise from the interaction with the low-frequency plasma.

The electromagnetic wave with *c*-axis polarization excites the transverse plasma which carries the oscillating current parallel to the *c* axis. When the frequency of the electromagnetic wave is smaller than the plasma frequency, the oscillating current is of a standing wave with a finite penetration depth from the crystal surface. On the other hand, when the frequency is larger than the plasma frequency, the current is of a propagating wave. Therefore, when the crystal has a finite thickness and a shape of film, the reflectivity and transmissivity of the electromagnetic wave strongly depend on the frequency and the thickness of the film. When the thickness of the film is relatively thick, e.g., 100 μm for $La_{1.84}Sr_{0.16}CuO_4$, the film almost perfectly reflects the electromagnetic wave with a frequency lower than the plasma frequency. When the frequency of the electromagnetic wave increases above the plasma frequency, the electromagnetic wave passes through the film in a form of the transverse plasma wave. As a result, the finite transmissivity appears and the reflectivity diminishes. In this frequency range, the reflectivity and transmissivity show an oscillatory frequency dependence which comes from the interference effect of the transverse plasma waves reflected at the film surfaces.

When the incident electromagnetic wave is unpolarized, the transmitted wave passing through the film is changed to the wave linearly polarized parallel to the *c* axis, since only the component of the electric field parallel to the *c* axis can pass through the film. Therefore, the film works as a polarizer.

An applied magnetic field strongly modifies the reflectivity and transmissivity. When vortices are introduced in the film by the magnetic field, the vortices have two kinds of effect changing the dielectric constant of the film. One is the effect of plasma damping due to the gapless excitation inside the vortex cores. The other is the effect of vortex motion driven by the oscillating current of the plasma. These effects act to decrease the reflectivity and transmissivity in the magnetic field.

The low-frequency plasma with *c*-axis polarization can be excited by the ac Josephson effect. A weak magnetic field is applied parallel to the junction barrier. In the Josephson junction with the barrier parallel to the oxide layers, two bulk plasmas with different wave numbers are excited when the Josephson frequency $\omega_0=2eV_0/\hbar$ exceeds the plasma frequency ω_{pc}. The Poynting vectors of the excited plasmas are almost parallel to the barrier. The maximum magnitude of the Poynting vector of one plasma appears at a Josephson frequency near ω_{pc} and that of the other plasma appears at a Josephson frequency near the transverse plasma frequency $\omega_T(q)$. In the process of the plasma decaying into electromagnetic wave, quite strong emission of the electromagnetic wave

propagating in the direction parallel to the oxide layers will be expected at the voltage corresponding to ω_{pc}. When the barrier is perpendicular to the oxide layers, the plasma whose Poynting vector is perpendicular to the barrier is excited by the ac Josephson effect. The magnitude of the Poynting vector has a maximum at a Josephson frequency above and near ω_{pc}. The plasma will emit the electromagnetic wave propagating perpendicular to the barrier in this junction.

The low-frequency plasma affects the *I-V* characteristics of the junction. When the junction barrier is parallel to the oxide layers, two peaks of the dc current appear in the *I-V* characteristics; one is at the voltage at which the ac Josephson current resonates with the Swihart wave[55] and the other is at the voltage at which the current resonates with the surface plasma around the barrier. When the junction barrier is perpendicular to the oxide layers, a peak of the dc current appears at the voltage corresponding to the Swihart wave frequency. There is no visible anomaly at the voltage corresponding to the surface plasma frequency in this junction.

Although we took $La_{2-x}Sr_xCuO_4$ as an example in the present paper, the electromagnetic phenomena discussed here are expected to be generally observed in all the cuprate superconductors with low-frequency plasma. It is known that the cuprates such as $Bi_2Sr_2CaSu_2O_8$ (Ref. 56) and oxygen-reduced $YBa_2Cu_3O_x$ (Ref. 2) also have low-frequency plasma.

ACKNOWLEDGMENTS

We would like to express sincere thanks to Professor S. Uchida, Professor K. Kitazawa, Professor T. Yamashita, Professor M. Ikezawa, Professor I. K. Schuller, Professor M. B. Maple, Professor H. Suhl, Professor K. Maki, and T. Sato for valuable discussions. This work is supported by a Grant-in-Aid for Scientific Research on Priority Area, "Science of High-T_c Superconductivity" given by the Ministry of Education, Science and Culture, Japan.

APPENDIX A: DIELECTRIC CONSTANT IN THE MIXED STATE

We derive the dielectric function of type-II superconductors in the mixed state within the London theory. In the following we confine ourselves to the isotropic case for simplicity. The extension to the anisotropic case is straightforward. In the London approximation the superconducting current and the charge are given by

$$\mathbf{J}(\mathbf{r},t)=-\frac{c}{4\pi\lambda_L^2}[\mathbf{A}(\mathbf{r},t)-\frac{\phi_0}{2\pi}\nabla\varphi(\mathbf{r},t)]\ , \tag{A1}$$

$$\rho(\mathbf{r},t)=-\frac{c^2}{4\pi\lambda_L^2 v_B^2}[A_0(\mathbf{r},t)+\frac{\phi_0}{2\pi}\frac{1}{c}\frac{\partial}{\partial t}\varphi(\mathbf{r},t)]\ , \tag{A2}$$

where $\mathbf{A}(\mathbf{r},t)$ and $A_0(\mathbf{r},t)$ are the vector potential and the scalar potential, respectively, $\varphi(\mathbf{r},t)$ is the phase of the superconducting order parameter, and v_B is the velocity of the Goldstone mode ($v_B=v_F/\sqrt{3}$, v_F being the Fermi velocity). The parameter μ in Eq. (5.3) is equal to $(v_B/c)\lambda_L$. From now on we use the notation $\partial_0\equiv(1/c)(\partial/\partial t)$ for brevity. We adopt the phason gauge for $(\mathbf{A}, A_0)$,[49]

$$\partial_0 A_0+\frac{v_B^2}{c^2}\nabla\cdot\mathbf{A}=0\ , \tag{A3}$$

and assume the phason equation

$$\left[\partial_0^2-\frac{v_B^2}{c^2}\nabla^2\right]\varphi=0\ . \tag{A4}$$

This gauge condition ensures the current conservation in the present system,

$$\frac{\partial}{\partial t}\rho+\nabla\cdot\mathbf{J}=0\ . \tag{A5}$$

Let us first calculate the longitudinal part of the dielectric function. The Maxwell equation ($\epsilon\nabla\cdot\mathbf{E}=4\pi\rho$) leads to the equation in the present system,

$$\epsilon\nabla\cdot\mathbf{E}=-\frac{c^2}{\lambda_L^2 v_B^2}\left[A_0+\frac{\phi_0}{2\pi}\partial_0\varphi\right]\ . \tag{A6}$$

Noting the relation, $\mathbf{E}=-\partial_0\mathbf{A}-\nabla A_0$, we find the equation for the scalar potential in the phason gauge from Eq. (A6),

$$\nabla A_0=\frac{v_B^2/c^2}{\partial_0^2-(v_B^2/c^2)\nabla^2}\nabla(\nabla\cdot\mathbf{E})-\frac{\phi_0}{2\pi}\nabla\partial_0\varphi\ . \tag{A7}$$

For the vector potential we have from Eq. (A1)

$$\partial_0\mathbf{A}=-\frac{4\pi\lambda_L^2}{c}\partial_0\mathbf{J}+\frac{\phi_0}{2\pi}\partial_0\nabla\varphi\ . \tag{A8}$$

From these equations it follows

$$\nabla\cdot\epsilon_L^M(\partial)\mathbf{E}=-\frac{\phi_0}{2\pi\lambda_L^2}\frac{1}{\partial_0^2}\nabla\cdot[\partial_0,\nabla]\varphi\ , \tag{A9}$$

where

$$\epsilon_L^M(\partial)=\epsilon+\frac{\lambda_L^{-2}}{\partial_0^2-(v_B^2/c^2)\nabla^2}\ , \tag{A10}$$

and $[A,B]=AB-BA$. In the Meissner state the right-hand side (rhs) of Eq. (A9) vanishes since the phase φ is a nonsingular (single-valued) function, i.e., the derivative operators acting on φ commute, so that, $\epsilon_L^M(\mathbf{k},\omega)$, which is defined as

$$\epsilon_L^M(\partial)\exp(i\mathbf{k}\cdot\mathbf{r}-i\omega t)=\epsilon_L^M(\mathbf{k},\omega)\exp(i\mathbf{k}\cdot\mathbf{r}-i\omega t)\ ,$$

is equal to the longitudinal dielectric function in the Meissner state,

$$\epsilon_L^M(\mathbf{k},\omega)=\epsilon-\frac{\omega_p^2}{\omega^2-v_B^2\mathbf{k}^2}\ , \tag{A11}$$

with $\omega_p^2=c^2/\lambda_L^2$. In the mixed state the rhs of Eq. (A9) is expressed in terms of the coordinates of the vortices. We consider the case where the vortices are directed in the y axis. We define the displacement field of the vortex lat-

tice, $\mathbf{u}(\mathbf{r},t)=(u_x(\mathbf{r},t),0,u_z(\mathbf{r},t))$,

$$\mathbf{u}(\mathbf{r},t)=\sum_i \mathbf{u}_i\delta^{(2)}(\mathbf{r}-\mathbf{R}_i^{(0)}) , \tag{A12}$$

where $\mathbf{u}_i$ is the displacement vector of the ith vortex and the summation is taken over the undistorted vortex lattice sites, $\mathbf{R}_i^{(0)}$. As shown in Appendix B, the commutator in Eq. (A9) is calculated to the linear in $\mathbf{u}$ as

$$[\partial_0,\nabla]\varphi(\mathbf{r},t)=2\pi\partial_0\mathbf{u}(\mathbf{r},t)\times\mathbf{e}_v=2\pi\begin{bmatrix}-\partial_0 u_z(\mathbf{r},t)\\0\\\partial_0 u_x(\mathbf{r},t)\end{bmatrix} , \tag{A13}$$

where $\mathbf{e}_v$ is the unit vector in the direction of the vortices. To relate the displacement field with the electromagnetic field we follow the calculation of the microwave penetration depth in the mixed state by Coffey and Clem.[42] We assume that the equation for $\mathbf{u}(\mathbf{r},t)$,

$$M\frac{\partial^2}{\partial t^2}\mathbf{u}+\eta\frac{\partial}{\partial t}\mathbf{u}+\kappa_p\mathbf{u}=\frac{B_0}{c}\mathbf{J}\times\mathbf{e}_v , \tag{A14}$$

where B_0 is the flux density, and M, η, and κ_p, are, respectively, the vortex inertial mass per unit length, the viscous drag coefficient, and the vortex pinning-force constant. This equation is solved as

$$\begin{aligned}u_x(\mathbf{r},t)&=\frac{B_0/4\pi}{M\partial_t^2+\eta\partial_t+\kappa_p}[-(\nabla\times\mathbf{H})_z+\epsilon\partial_0 E_z],\\ u_z(\mathbf{r},t)&=\frac{B_0/4\pi}{M\partial_t^2+\eta\partial_t+\kappa_p}[(\nabla\times\mathbf{H})_x-\epsilon\partial_0 E_x] ,\end{aligned} \tag{A15}$$

with $\partial_t\equiv\partial/\partial t$. Thus, Eqs. (A13) and (A15) lead to the relation,

$$\nabla\cdot[\partial_0,\nabla]\varphi=\frac{\epsilon B_0/2}{M\partial_t^2+\eta\partial_t+\kappa_p}\partial_0^2(\partial_x E_x+\partial_z E_z) . \tag{A16}$$

Substituting Eq. (A16) into Eq. (A9), we have the longitudinal dielectric function in the vortex lattice state, which is an anisotropic tensor because of the existence of the vortices as follows:

$$\epsilon_L^{xx}(\mathbf{k},\omega)=\epsilon_L^{zz}(\mathbf{k},\omega)=\epsilon_L^{M}(\mathbf{k},\omega)+\frac{\phi_0}{4\pi\lambda_L^2}\frac{\epsilon B_0}{\kappa_p-i\eta\omega-M\omega^2} , \tag{A17}$$

$$\epsilon_L^{yy}(\mathbf{k},\omega)=\epsilon_L^{M}(\mathbf{k},\omega) . \tag{A18}$$

The off-diagonal components vanish in the present coordinates.

Let us next calculate the transverse dielectric function. The Maxwell equation, $\nabla\times\mathbf{H}=(4\pi/c)\mathbf{J}+\epsilon\partial_0\mathbf{E}$, in the present system is expressed as

$$\nabla\times\mathbf{H}=T(\nabla)\left[-\frac{1}{\lambda_L^2}\left[\mathbf{A}-\frac{\phi_0}{2\pi}\nabla\varphi\right]+\epsilon\partial_0\mathbf{E}\right] , \tag{A19}$$

where $T(\nabla)=(T_{ij}(\nabla))$ is the projection operator defined as

$$T_{ij}(\nabla)=\delta_{ij}-\frac{\nabla_i\nabla_j}{\nabla^2} . \tag{A20}$$

The time derivative of the rhs of Eq. (A19) is easily obtained in the form

$$\begin{aligned}&\partial_0\left[-\frac{1}{\lambda_L^2}\left[\mathbf{A}-\frac{\phi_0}{2\pi}\nabla\varphi\right]+\epsilon\partial_0\mathbf{E}\right]\\&=\partial_0^2\epsilon_T^M(\partial)T(\nabla)\mathbf{E}+\partial_0^2\epsilon_L^M(\partial)L(\nabla)\mathbf{E}\\&\quad+\frac{\phi_0}{2\pi\lambda_L^2}[\partial_0,\nabla]\varphi ,\end{aligned} \tag{A21}$$

where $L(\nabla)$ is the projection operator defined as

$$L_{ij}(\nabla)=\frac{\nabla_i\nabla_j}{\nabla^2} , \tag{A22}$$

and $\epsilon_T^M(\partial)$ is the transverse dielectric function in the Meissner state,

$$\epsilon_T^M(\partial)=\epsilon+\frac{\lambda_L^{-2}}{\partial_0^2} . \tag{A23}$$

In deriving Eq. (A21) use was made of Eq. (A7). Noting relations (A13) and (A15), we obtain the following equation for the oscillatory part of the rhs of Eq. (A19) from Eq. (A21):

$$\begin{aligned}&T(\nabla)\left[-\frac{1}{\lambda_L^2}\left[\mathbf{A}-\frac{\phi_0}{2\pi}\nabla\varphi\right]+\epsilon\partial_0\mathbf{E}\right]_{\rm osc}\\&=-\nabla\times\left[\frac{\phi_0}{4\pi\lambda_L^2}\frac{B_0}{M\partial_t^2+\eta\partial_t+\kappa_p}\hat{V}\mathbf{H}\right]\\&\quad+\partial_0\left[\epsilon_T^M(\partial)+\frac{\phi_0}{4\pi\lambda_L^2}\frac{B_0}{M\partial_t^2+\eta\partial_t+\kappa_p}\hat{U}\right]T(\nabla)\mathbf{E} ,\end{aligned} \tag{A24}$$

where $\hat{V}$ and $\hat{U}$ are matrices defined by

$$\hat{V}=\begin{bmatrix}0&0&0\\0&1&0\\0&0&0\end{bmatrix},\quad \hat{U}=\begin{bmatrix}1&0&0\\0&0&0\\0&0&1\end{bmatrix} . \tag{A25}$$

In Eq. (A24), $\mathbf{E}$ and $\mathbf{H}$ are assumed independent of y. Substituting Eq. (A24) into Eq. (A19), we can rewrite Eq. (A19) in the form

$$\nabla\times\mathbf{H}=\hat{\epsilon}_T(\partial)\partial_0 T(\nabla)\mathbf{E} , \tag{A26}$$

where $\hat{\epsilon}(\partial)$ is the transverse dielectric tensor. Their nonvanishing components are given by

$$\epsilon_T^{xx}(\omega)=\epsilon_T^{zz}(\omega)=\epsilon-\frac{\omega_{ps}^2}{\omega(\omega+i0^+)}\left[1+\frac{\phi_0}{4\pi\lambda_L^2}\frac{B_0}{\kappa_p-i\eta\omega-M\omega^2}\right]^{-1} , \tag{A27}$$

$$\epsilon_T^{yy}(\omega)=\epsilon-\frac{\omega_{ps}^2}{\omega(\omega+i0^+)} . \tag{A28}$$

In the configurations given in Sec. IV, Eq. (A26) is reduced to

$$\frac{\partial}{\partial x}H_y(x,\omega)=\left\{\epsilon-\frac{\omega_{ps}^2}{\omega(\omega+i0^+)}\times\left[1+\frac{\phi_0}{4\pi\lambda_L^2}\frac{B_0}{\kappa_p-i\eta\omega-M\omega^2}\right]^{-1}\right\}\times\partial_0 E_z(x,\omega)\ . \tag{A29}$$

When the contribution of the normal current is further included in the system on the basis of the two-fluid model and also the anisotropy of the penetration depth is considered, Eq. (A29) is extended to the following form:

$$\frac{\partial}{\partial x}H_y(x,\omega)=\left\{\epsilon-\left[\frac{\omega_{ps}^2}{\omega(\omega+i0^+)}+\frac{\omega_{pn}^2}{\omega(\omega+i\gamma)}\right]\times\left[1+\frac{\phi_0}{4\pi\lambda_c^2}\frac{B_0}{\kappa_p-i\eta\omega-M\omega^2}\right]^{-1}\right\}\times\partial_0 E_z(x,\omega)\ , \tag{A30}$$

where λ_c is the penetration depth associated with the current flowing along the c axis.

APPENDIX B: DERIVATION OF EQS. (A13), (4.4), AND (4.5)

When the phase $\varphi(\mathbf{r},t)$ has a topological singularity, i.e., $\varphi(\mathbf{r},t)$ is a multivalued function, the differential operations on $\varphi(\mathbf{r},t)$ do not commute generally. The general and complete theory for the topological singularity is given in Ref. 49. The commutation relations of the differential operators acting on $\varphi(\mathbf{r},t)$ can be calculated on the basis of this theory. In this Appendix we give a brief description of Eqs. (A13), (4.4), and (4.5). In the following we use the notations, $(ct,\mathbf{r})=(x_0,x_1,x_2,x_3)$ for the coordinates, and $\partial_\mu=\partial/\partial x_\mu$ for the differential operators ($\mu=0,1,2,3$).

1. Derivation of Eq. (A13)

Consider a moving vortex. We assumed that the coordinates of the vortex line are described by an equation of two parameters τ and σ, $(-\infty<\tau,\sigma<\infty)$,

$$x_0=\tau,\ x_1=R_1(\tau,\sigma),\ x_2=\sigma,\ x_3=R_3(\tau,\sigma)\ , \tag{B1}$$

where $R_1(\tau,\sigma)$ and $R_3(\tau,\sigma)$ are arbitrary functions. Here we assumed that the vortex line is extended from $-\infty$ to ∞ in the x_2 direction. Note that this is the equation of a surface in the 4D space. We start with the integral relation

$$\oint_C\sum_\mu dx_\mu\partial_\mu\varphi=\frac{1}{2}\int_S\sum_{\mu,\nu}dx_\mu dx_\nu[\partial_\mu,\partial_\nu]\varphi\ , \tag{B2}$$

where the path C is a closed line in the 4D space $(x_0,\ldots,x_3)$ and S is a surface enclosed by the line C. In the integral on the rhs of Eq. (B2) the relation, $dx_\mu dx_\nu=-dx_\nu dx_\mu$, is assumed. Consider the 3D space (x_3,x_1,x_0) with a fixed value of x_2. In this space Eq. (B1) is reduced to the equation of a line extended from $-\infty$ to ∞ in the x_0 direction,

$$x_3=R_3(\tau,x_2),\ \ x_1=R_1(\tau,x_2),\ \ x_0=\tau\ . \tag{B3}$$

We take the path C along a closed line inside this 3D space. Equation (B2) is then written as

$$\oint_C\sum_{\mu=3,1,0}dx_\mu\partial_\mu\varphi=\int_S\{dx_1dx_0[\partial_1,\partial_0]\varphi+dx_0dx_3[\partial_0,\partial_3]\varphi+dx_3dx_1[\partial_3,\partial_1]\varphi\}\ . \tag{B4}$$

The value of the line integral is equal to 2π when the closed path C enclosed the line (B3) and otherwise it vanishes. It is noted that the relation (B4) has exactly the same structure as that of the integral relation ($\oint d\mathbf{r}\cdot\nabla\varphi=\int d\mathbf{S}\cdot\nabla\times\nabla\varphi$) for the phase of a static vortex state in the 3D space, (x_1,x_2,x_3). Since the commutators, $[\partial_i,\partial_j]\varphi$ $(i,j=0,1,3)$, do not vanish only on the line (B3), they should have the form

$$[\partial_i,\partial_j]\varphi\propto\delta(x_1-R_1(x_0,x_2))\delta(x_3-R_3(x_0,x_2))\ , \tag{B5}$$

in order that the surface integral in Eq. (B4) gives a finite value. By analogy with the vector, $\nabla\times\nabla\varphi$, in the (x_1,x_2,x_3) space, it is reasonable to assume that the vector,

$$\mathbf{g}=\begin{bmatrix}[\partial_1,\partial_0]\varphi\\ [\partial_0,\partial_3]\varphi\\ [\partial_3,\partial_1]\varphi\end{bmatrix} \tag{B6}$$

is parallel to the tangential vector of the line (B3), $(\partial R_3/\partial\tau,\partial R_1/\partial\tau,1)$,[49,57] so that we have

$$\begin{aligned}&[\partial_1,\partial_0]\varphi=2\pi\partial_0R_3(x_0,x_2)\delta(x_1-R_1(x_0,x_2))\delta(x_3-R_3(x_0,x_2))\ ,\\ &[\partial_0,\partial_3]\varphi-2\pi\partial_0R_1(x_0,x_2)\delta(x_1-R_1(x_0,x_2))\delta(x_3-R_3(x_0,x_2))\ ,\\ &[\partial_3,\partial_1]\varphi=2\pi\delta(x_1-R_1(x_0,x_2))\delta(x_3-R_3(x_0,x_2))\ .\end{aligned} \tag{B7}$$

It is easy to check that Eq. (B7) leads to the correct value of the integral (B4), 2π. For example, take a closed path C on the x_1-x_0 plane. Then, the surface integral in Eq. (B4) is calculated as

$$\int_S dx_1dx_0[\partial_1,\partial_0]\varphi=2\pi\int dx_0\partial_0R_3(x_0,x_2)\delta(x_3-R_3(x_0,x_2))=2\pi\ . \tag{B8}$$

Equation (B7) in the single vortex state is extended in the vortex lattice state as follows:

$$[\partial_1,\partial_0]\varphi=2\pi\sum_i \partial_0 R_{3i}(x_0,x_2)\delta^{(2)}[\mathbf{r}-\mathbf{R}_i(x_0,x_2)] ,$$
$$[\partial_0,\partial_3]\varphi=2\pi\sum_i \partial_0 R_{1i}(x_0,x_2)\delta^{(2)}[\mathbf{r}-\mathbf{R}_i(x_0,x_2)] , \tag{B9}$$
$$[\partial_3,\partial_1]\varphi=2\pi\sum_i \delta^{(2)}[\mathbf{r}-\mathbf{R}_i(x_0,x_2)] ,$$

where $\mathbf{r}=(x_3,x_1)$ and $\mathbf{R}_i=(R_{3i},R_{1i})$. The summation with respect to i is taken over the vortex sites. In the case of a deformed vortex lattice, introducing the displacement vector of the ith vortex $\mathbf{u}_i=[u_{3i}(x_0,x_2),u_{1i}(x_0,x_2)]$, we may write $\mathbf{R}_i$ as

$$\mathbf{R}_i(x_0,x_2)=\mathbf{R}_i^{(0)}+\mathbf{u}_i(x_0,x_2) , \tag{B10}$$

where $\mathbf{R}_i^{(0)}$ denotes the ith regular lattice site. Substituting (B10) into (B9), we have in the linear approximation

$$[\partial_0,\partial_1]\varphi=-2\pi\partial_0 u_3(t,\mathbf{r}),\quad [\partial_0,\partial_3]\varphi=2\pi\partial_0 u_1(t,\mathbf{r}) , \tag{B11}$$

where

$$u_\alpha(t,\mathbf{r})=\sum_i u_{\alpha i}\delta^{(2)}(\mathbf{r}-\mathbf{R}_i^{(0)}) . \tag{B12}$$

2. Derivation of Eqs. (4.4) and (4.5)

Let us consider a Josephson junction in which the junction barrier with an infinitesimal width is placed at $x_3=0$. The phase $\varphi(\mathbf{r},t)$ then has a discontinuity at $x_3=0$ when a magnetic field or a voltage is applied in the region of the junction. We evaluate the line integral (B2) along a closed path C on the (x_α,x_3) plane, where $\alpha=1$ or 0, with fixed values of the other coordinates, which we denote x_β. In this case Eq. (B2) is reduced to

$$\oint_C \sum_{\mu=\alpha,3} dx_\mu\partial_\mu\varphi=\int_S dx_3 dx_\alpha[\partial_3,\partial_\alpha]\varphi(x_\alpha,x_3,x_\beta) . \tag{B13}$$

The path C is assumed to cross the line $x_3=0$ at $x_\alpha=a$ and $b(a<b)$ on this plane. We divide the path C into two parts, C_1 and C_2, where the path $C_1(C_2)$ is the part of C in the region of $x_3<0$ ($x_3>0$). In this case the line integral in Eq. (B13) is obtained from the sum of the two parts, $I^{(1)}$ and $I^{(2)}$,

$$\oint_C \sum_{\mu=\alpha,3} dx_\mu\partial_\mu\varphi=I^{(1)}+I^{(2)} , \tag{B14}$$

where

$$I^{(l)}=\int_{C_l} dx_\mu\partial_\mu\varphi , \tag{B15}$$

with $l=1$ or 2. Consider the integrals along the lines parallel to $x_3=0$ from a to b ($\{a,b\}$) and from b to a ($\{b,a\}$),

$$K^{(1)}=\int_a^b dx_\alpha\partial_\alpha\varphi(x_\alpha,x_3=-\varepsilon,x_\beta) , \tag{B16}$$
$$K^{(2)}=\int_b^a dx_\alpha\partial_\alpha\varphi(x_\alpha,x_3=+\varepsilon,x_\beta) , \tag{B17}$$

where ε is an infinitesimal positive number. It is noted that the paths, $C_1+\{a,b\}$ and $C_2+\{b,a\}$ form closed lines. Since no singular point exists inside the regions enclosed by the lines, we have the relations, $I^{(1)}+K^{(1)}=0$ and $I^{(2)}+K^{(2)}=0$. The integral (B14) is, therefore, calculated as

$$\oint_C \sum_{\mu=\alpha,3} dx_\mu\partial_\mu\varphi=-K^{(1)}-K^{(2)} =\chi(b,x_\beta)-\chi(a,x_\beta) . \tag{B18}$$

Here, $\chi(x,x_\beta)$ is the phase difference at the barrier,

$$\chi(x,x_\beta)\equiv\lim_{\varepsilon\to 0}\{\varphi(x,x_3=+\varepsilon,x_\beta) -\varphi(x,x_3=-\varepsilon,x_\beta)\} . \tag{B19}$$

In order that the surface integral in Eq. (B13) gives the result (B18), the commutator in the integrand should be equal to

$$[\partial_3,\partial_\alpha]\varphi(x_\alpha,x_3,x_\beta)=\partial_\alpha\chi(x_\alpha,x_\beta)\delta(x_3) . \tag{B20}$$

Thus we have the relations,

$$[\partial_3,\partial_0]\varphi(x_0,x_1,x_3)=\partial_0\chi(x_0,x_1)\delta(x_3) , \tag{B21}$$
$$[\partial_3,\partial_1]\varphi(x_0,x_1,x_3)=\partial_1\chi(x_0,x_1)\delta(x_3) . \tag{B22}$$

APPENDIX C: TOTAL TUNNELING CURRENT ACROSS THE JUNCTION BARRIER PERPENDICULAR TO THE OXIDE LAYERS

In this Appendix we calculate the total tunneling current of $O(J_c^2)$. To simplify the problem we consider the case where the single-electron current can be neglected, that is, $R\to\infty(Q\to\infty)$. The dc Josephson current given by Eqs. (4.50) and (4.51) may be considered as a quantity of $O(J_c^2)$ when the Josephson critical current J_c is small [Note that $\lambda_J^{-2}\sim O(J_c)$ as seen in Eq. (4.30)]. Then, we evaluate the displacement current up to the order of J_c^2 in the following. Since the displacement current is related to $\theta(x,t)$ as

$$C\frac{\partial}{\partial t}V(x,t)=\frac{\phi_0 c}{16\pi^2\lambda_a}\frac{1}{\bar{c}^2}\frac{\partial^2}{\partial t^2}\theta(x,t)\ , \tag{C1}$$

the phase difference of $O(J_c^2),\theta^{(2)}(x,t)$, gives the displacement current of $O(J_c^2)$. [Note that the solutions given in Eqs. (4.29) and (4.43) are $O(J_c)$]. If $\theta^{(2)}(x,t)$ contains a term proportional to t^2, the displacement current has a dc part of $O(J_c^2)$. The equation for $\theta^{(2)}(x,t)$ is derived from Eq. (4.22) as follows,

$$\int dx'\int dt' K(x-x',t-t')\frac{\partial^2}{\partial x'^2}\theta^{(2)}(x',t')-\frac{1}{\bar{c}^2}\frac{\partial^2}{\partial t^2}\theta^{(2)}(x,t)=\frac{16\pi^2\lambda_a}{\phi_0 c}J_c\cos(qx+\omega_0 t)\theta^{(1)}(x,t)\ , \tag{C2}$$

where $\theta^{(1)}(x,t)$ is the solution of $O(J_c)$

$$\theta^{(1)}(x,t)=\frac{16\pi^2\lambda_a}{\phi_0 c}\frac{\bar{c}^2}{\omega_0^2}\frac{J_c}{[1-(\bar{c}^2q^2/\omega_0^2)K_1(q,\omega_0)]^2+[(\bar{c}^2q^2/\omega_0^2)K_2(q,\omega_0)]^2}$$
$$\times\left\{\frac{\bar{c}^2q^2}{\omega_0^2}K_2(q,\omega_0)\cos(qx+\omega_0 t)+\left[1-\frac{\bar{c}^2q^2}{\omega_0^2}K_1(q,\omega_0)\right]\sin(qx+\omega_0 t)\right\}\ . \tag{C3}$$

Note that $K_1(q,\omega_0)\neq 0, K_2(q,\omega_0)=0$ for $\omega_0<\omega_{pc}$ or $\omega_0>\omega_T(q)$ and $K_1(q,\omega_0)=0$, $K_2(q,\omega_0)\neq 0$ for $\omega_{pc}<\omega_0<\omega_T(q)$. When Eq. (C3) is substituted into Eq. (C2), the rhs of Eq. (C2) generates a dc part in the case of $\omega_0>\omega_T(q)$ which is a contribution of the cosine term in Eq. (C3),

$$\frac{16\pi^2\lambda_a}{\phi_0 c}J_c\cos(qx+\omega_0 t)\theta^{(1)}(x,t)$$
$$=\left[\frac{16\pi^2\lambda_a}{\phi_0 c}\right]^2\frac{\bar{c}^2}{2\omega_0^2}\frac{J_c^2(\bar{c}^2q^2/\omega_0^2)K_2(q,\omega_0)}{[1-(\bar{c}^2q^2/\omega_0^2)K_1(q,\omega_0)]^2+[(\bar{c}^2q^2/\omega_0^2)K_2(q,\omega_0)]^2}+\text{ac part}\ . \tag{C4}$$

Equation (C2), then, has a solution of the form

$$\theta^{(2)}(x,t)=\left[\frac{16\pi^2\lambda}{\phi_0 c}\right]^2\frac{1}{2\omega_0^2}\frac{J_c^2(\bar{c}^2q^2/\omega_0^2)K_2(q,\omega_0)}{[1-(\bar{c}^2q^2/\omega_0^2)K_1(q,\omega_0)]^2+[(\bar{c}^2q^2/\omega_0^2)K_2(q,\omega_0)]^2}$$
$$\times[ax^2-(1-a)\bar{c}^2t^2]+\cdots\ , \tag{C5}$$

where $\cdots$ stands for the oscillatory terms and a is a number which depends on the details of the circuit including the Josephson junction. This solution gives the dc displacement current when $\hbar\omega_{pc}/2e<V_0<\hbar\omega_T(q)/2e$,

$$\left[\frac{1}{C}\frac{\partial}{\partial t}V(x,t)\right]_{\text{dc}}=-(1-a)J_c\frac{\bar{c}^2}{2\lambda_J^2\omega_0^2}\left[\frac{(\bar{c}^2q^2/\omega_0^2)}{\sqrt{(\omega_0^2/\omega_c^2)-\lambda_c^2q^2-1}}\right]\left[1+\left[\frac{(\bar{c}^2q^2/\omega_0^2)}{\sqrt{(\omega_0^2/\omega_c^2)-\lambda_c^2q^2-1}}\right]^2\right]^{-1}\ , \tag{C6}$$

and the total current in this case is obtained as

$$I_{\text{total}}=aJ_c\frac{\bar{c}^2}{2\lambda_J^2\omega_0^2}\left[\frac{(\bar{c}^2q^2/\omega_0^2)}{\sqrt{(\omega_0^2/\omega_c^2)-\lambda_c^2q^2-1}}\right]\left[1+\left[\frac{(\bar{c}^2q^2/\omega_0^2)}{\sqrt{(\omega_0^2/\omega_c^2)-\lambda_c^2q^2-1}}\right]^2\right]^{-1}\ . \tag{C7}$$

When a is positive, the total current is positive irrespective of the sign of the dc Josephson current.

[1] K. Tamasaku, Y. Nakamura, and S. Uchida, Phys. Rev. Lett. **69**, 1455 (1992).

[2] C. C. Homes, T. Timusk, R. Liang, D. A. Bonn, and W. N. Hardy, Phys. Rev. Lett. **71**, 1645 (1993).

[3] S. Tajima, S. Uchida, H. Ishii, H. Takagi, S. Tanaka, U. Kawabe, H. Hasegawa, T. Aita, and T. Ishiba, Mod. Phys. Lett. **1**, 353 (1988).

[4] S. Uchida, T. Ido, H. Takagi, T. Arima, Y. Tokura, and S. Tajima, Phys. Rev. B **43**, 7942 (1991).

[5] F. Gao, D. B. Romero, D. B. Tanner, J. Talvacchio, and M. G. Forrester, Phys. Rev. B **47**, 1036 (1993).

[6] Y. J. Uemura *et al.* Phys. Rev. Lett. **62**, 2317 (1989).

[7] J. Orenstein, G. A. Thomas, A. J. Millis, S. L. Cooper, D. H. Rapkine, T. Timusk, L. F. Schneemeyer, and J. V. Waszczak, Phys. Rev. B **42**, 6342 (1990).

[8] H. P. Geserich, B. Koch, M. Dürrler, and Th. Wolf, in *Electronic Properties of High-T_c Superconductors and Related Compounds*, edited by H. Kuzmany, M. Mehring, and J. Fink, Springer Series in Solid State Physics Vol. 99 (Springer-Verlag, Berlin, 1990), p. 265; B. Koch, M. Dürrler, H. P. Geserich, Th. Wolf, G. Roth, and G. Zachmann, *ibid.*, p. 290.

[9] N. Nücker, H. Romberg, S. Nakai, B. Scheerer, J. Fink, Y. F. Yan, and Z. X. Zhao, Phys. Rev. B **39**, 12 379 (1989).

[10]C. T. Chen, L. H. Tjeng, J. Kwo, H. L. Kao, P. Ludolf, F. Sette, and R. M. Fleming, Phys. Rev. Lett. **68**, 2543 (1992).
[11]T. Hasegawa, M. Nantoh, H. Ikuta, and K. Kitazawa, Physica C **185-189**, 1743 (1991).
[12]R. Kleiner, F. Steinmeyer, G. Kunkel, and P. Müller, Phys. Rev. Lett. **68**, 2394 (1992).
[13]K. Kadowaki, in *Proceedings of the International Workshop on Electronic Properties and Mechanisms in High-T_c Superconductors*, edited by T. Oguchi, K. Kadowski, and T. Sasaki (North-Holland, Amsterdam, 1992), p. 209.
[14]S. Martin, A. T. Fiory, R. M. Fleming, L. F. Schneemeyer, and J. V. Waszczak, Phys. Rev. Lett. **60**, 2194 (1988); Phys. Rev. B **41**, 846 (1990).
[15]T. Ito, H. Takagi, S. Ishibashi, T. Ido, and S. Uchida, Nature (London) **350**, 596 (1991).
[16]H. L. Kao, J. Kwo, H. Takagi, and B. Batlogg, Phys. Rev. B **48**, 9925 (1993).
[17]Y. Iye, in *Properties of High-Temperature Superconductors III*, edited by D. M. Ginsberg (World Scientific, Singapore, 1992), p. 285.
[18]X.-D. Xiang, W. A. Vareka, A. Zettl, J. L. Corkill, M. L. Cohen, N. Kijima, and R. Gronsky, Phys. Rev. Lett. **68**, 530 (1992).
[19]P. W. Anderson, Phys. Rev. Lett. **67**, 3844 (1991).
[20]N. Nagaosa and P. A. Lee, Phys. Rev. Lett. **64**, 2450 (1990).
[21]H. Fukuyama, Prog. Theor. Phys., Suppl. **108**, 287 (1992).
[22]S. Chakravarty, A. Sudbø, P. W. Anderson, and S. Strong, Science **261**, 337 (1993).
[23]S. Massidda, J. Yu, and A. J. Freeman, Physica C **152**, 251 (1988).
[24]W. E. Pickett, R. E. Cohen, and H. Krakauer, Phys. Rev. B **42**, 8764 (1990).
[25]O. K. Andersen, A. I. Liechtenstein, O. Rodriguez, I. I. Mazin, O. Jepsen, V. P. Antropov, O. Gunnarsson, and S. Gopalan, Physica C **185-189**, 147 (1991).
[26]M. Tachiki, S. Takahashi, F. Steglich, and H. Adrian, Z. Phys. B **80**, 161 (1990); M. Tachiki, T. Koyama, and S. Takahashi, Physica C **185-189**, 303 (1991).
[27]L. N. Bulaevskii, M. Ledvij, and V. G. Kogan, Phys. Rev. B **46**, 366 (1992).
[28]T. Schneider and M. P. Sorensen, Z. Phys. B **80**, 331 (1990).
[29]A. A. Abrikosov, Physica C **182**, 191 (1991).
[30]R. A. Klemm and S. H. Liu, Phys. Rev. B **44**, 7526 (1991).
[31]R. Côté and A. Griffin, Phys. Rev. B **48**, 10 404 (1993).
[32]V. Z. Kresin and H. Morawitz, Phys. Rev. B **37**, 7854 (1988).
[33]H. A. Fertig and S. D. Sarma, Phys. Rev. B **43**, 4480 (1991).
[34]S. Doniach and M. Inui, Phys. Rev. B **41**, 6668 (1990).
[35]D. Reagor, E. Ahrens, S-W. Cheong, A. Migliori, and Z. Fisk, Phys. Rev. Lett. **62**, 2048 (1989).
[36]G. Cao, J. W. O'Reilly, J. E. Crow, and L. R. Testardi, Phys. Rev. B **47**, 11 510 (1993).
[37]L. Pintschovius, N. Pyka, W. Reichardt, A. Y. Rumiantsev, N. L. Mitrofanov, A. S. Ivanov, G. Collin, and P. Bourges, Physica C **185-189**, 156 (1991).
[38]D. van der Marel, H.-U. Harbermeier, D. Heitmann, W. König, and A. Wittlin, Physica C **176**, 1 (1991).
[39]R. T. Collins, Z. Schlesinger, F. Holtzberg, and C. Feidl, U. Welp, G. W. Crabtree, J. Z. Liu, and Y. Fang, Phys. Rev. B **43**, 8701 (1991).
[40]M. Tinkham, *Introduction to Superconductivity* (McGraw-Hill, New York, 1975).
[41]L. D. Landau, E. M. Lifshitz, and L. P. Pitaevskii, *Electrodynamics of Continuous Media* (Pergamon, Oxford, 1984), p. 293.
[42]M. W. Coffey and J. R. Clem. Phys. Rev. Lett. **67**, 386 (1991).
[43]E. H. Brandt, Phys. Rev. Lett. **67**, 2219 (1991).
[44]N. C. Yeh, Phys. Rev. B **43**, 523 (1991).
[45]G. Blatter, M. V. Feigel'man, A. I. Larkin, and V. M. Vinokur (unpublished).
[46]M. Golosovsky, Y. Naveh, and D. Davidov, Phys. Rev. B **45**, 7495 (1992).
[47]J. Owliaei, S. Sridhar, and J. Talacchio, Phys. Rev. Lett. **69**, 3366 (1992).
[48]J. Bardeen and M. J. Stephen, Phys. Rev. **140**, A1197 (1965).
[49]H. Umezawa, H. Matsumoto, and M. Tachiki, *Thermo Field Dynamics and Condensed States* (North-Holland, Amsterdam, 1982).
[50]F. Mancini, H. Matsumoto, M. Wadati, and H. Umezawa, Prog. Theor. Phys. **62**, 12 (1976).
[51]Since the electromagnetic field is expressed in terms of a retarded function, the square root of $Z'(q,\omega_0)$ is defined as $\sqrt{Z'(q,\omega_0)}=\sqrt{|\lambda_3^2q^2+1-(\omega_0^2/\omega_p^2)|}[\Theta(\omega_T(q)-\omega_0)+i\Theta(\omega_-\omega_T(q))]$, $\Theta(\omega)$ being the step function.
[52]A. Barone and G. Paternó, *Physics and Applications of the Josephson Effects* (Wiley, New York, 1982).
[53]A. A. Abrikosov, *Fundamental of the Theory of Metals* (North-Holland, Amsterdam, 1988).
[54]J. C. Swihart, J. Appl. Phys. **32**, 461 (1961).
[55]R. E. Eck, D. J. Scalapino, and B. N. Taylor, Phys. Rev. Lett. **13**, 15 (1964).
[56]S. Tajima, G. D. Gu, S. Miyamoto, A. Odagawa, and N. Koshizuka, Phys. Rev. B **48**, 16 164 (1993).
[57]E. H. Brandt, J. Low. Temp. Phys. **28**, 263 (1977).